NATIONAL ADVISORY COMMITTEE FOR AERONAUTICS

TECHNICAL NOTE 3066

EFFECT OF SURFACE ROUGHNESS OVER THE DOWNSTREAM REGION OF A 23° CONICAL DIFFUSER

By Jerome Persh and Bruce M. Bailey

Langley Aeronautical Laboratory
Langley Field, Va.

Washington
January 1954

NATIONAL ADVISORY COMMITTEE FOR AERONAUTICS

TECHNICAL NOTE 3066

EFFECT OF SURFACE ROUGHNESS OVER THE DOWNSTREAM REGION OF A 23° CONICAL DIFFUSER

By Jerome Persh and Bruce M. Bailey

SUMMARY

An experimental investigation was conducted to determine the effects of varying extents of surface roughness over the downstream region of a 23° conical diffuser having an inlet-boundary-layer thickness of the order of 5 percent of the inlet diameter. The air flows used in this investigation cover an inlet Mach number range from about 0.10 to 0.40 corresponding to Reynolds numbers of approximately 1×10^6 to 4×10^6 based on inlet diameter. The surface roughening was accomplished by coating the surface of the diffuser with graded cork particles of a controlled size. Incremental bands of roughness were removed from the upstream end (a 1-inch-wide band being retained near the inlet to stabilize the flow) after each series of pressure measurements was made so that the variation of diffuser performance with percent of diffuser length roughened could be determined.

The results of the present investigation and those of NACA RM L51K09 indicate that the flow in the roughened diffuser was steady and reproducible for all conditions. The values of total-pressure-loss coefficient measured at both the tailpipe exit and diffuser exit for the almost fully roughened diffuser were found to be 8 and 21 percent lower, respectively, than the value of total-pressure-loss coefficient for the smooth-surface diffuser measured at the tailpipe exit.

INTRODUCTION

Reference 1 indicated that, although the static-pressure recovery of a short, wide-angle diffuser was barely affected as a result of either roughening almost the entire surface of the diffuser or installing a roughness strip near the diffuser inlet, the flow pattern was considerably improved over that found in the same diffuser without any roughness. This encouraging result suggested that, since a steady symmetrical flow pattern could be achieved by using surface roughness, possible gains in

diffuser performance might be realized by judicious placement of the areas of surface roughness.

The skin friction in the upstream region of a diffuser probably contributes more to the overall total-pressure losses than does the skin friction in the downstream region because the boundary layer approaches a separated condition as it flows toward the diffuser exit, with an accompanying decrease in skin-friction coefficient. Speculation that the performance of the almost fully roughened diffuser (ref. 1) might be improved by decreasing the skin friction in the upstream region of the diffuser, consequently, led to the expediency of increasing the extent of smooth surface in this region. By retaining the roughness strip near the diffuser inlet, this procedure could be accomplished without sacrificing the flow stability.

The present investigation was therefore undertaken as a continuation of the investigation of reference 1 to determine whether gains in diffuser performance could be attained through the judicious use of continuous surface roughness. The results of the present investigation, in which the variation of diffuser performance with extent of roughness increasing from the diffuser exit in an upstream direction is determined, are directly comparable with the results of reference 1, in which the variation of diffuser performance was studied with extent of roughness increasing from a point near the inlet in a downstream direction, because essentially the same apparatus was used for both investigations and the thickness and shape factors of the inlet boundary layer were the same for both experiments.

The data presented herein cover an inlet Mach number range from about 0.10 to 0.40 corresponding to Reynolds numbers of approximately 1×10^6 to 4×10^6 based on inlet diameter. The extent of roughness over the downstream region of the diffuser was varied so that the variation of diffuser performance with percent of diffuser length roughened could be computed. Boundary-layer velocity profiles are presented for all roughness configurations as obtained from measurements at the diffuser inlet station, several longitudinal points in the diffuser, the diffuser exit, and the tailpipe exit.

SYMBOLS

g	acceleration due to gravity, ft/sec^2
h	total pressure, lb/sq ft
$\bar{h}$	weighted mean value of total pressure, lb/sq ft

$\Delta\bar{h}$	weighted-total-pressure loss from pressure surveys, lb/sq ft
L	diffuser length, in.
M	Mach number
p	static pressure, lb/sq ft
Δp	wall static-pressure rise, lb/sq ft
Δp_{ideal}	static-pressure rise for frictionless, incompressible, one-dimensional flow with same entering mass flow and geometric area, lb/sq ft
P_0	barometric pressure, in. Hg
T_0	stagnation temperature, $^{\circ}R$
q_c	impact pressure, $\bar{h} - p$, lb/sq ft
r	radial distance from center line, in.
R	radius, in.
R_e	Reynolds number based on inlet diameter, $2\frac{\rho UR}{\mu}$
u	local velocity at any point, ft/sec
U	local velocity at edge of boundary layer, ft/sec
u/U	velocity ratio, $\sqrt{\frac{h - p}{h_{max} - p}}$
W_s	standardized weight flow, $\frac{29.92}{P_0}\sqrt{\frac{T_0}{520}}\,2\pi g\int_0^R \rho ur\,dr$, lb/sec
x	distance along longitudinal axis measured from inlet, station 1, in.
y	perpendicular distance from diffuser wall, in.
μ	viscosity, lb-sec/ft^2

ρ mass density, lb-sec^2/ft^4

δ boundary-layer thickness, equal to y for $\frac{u}{U} = 0.95$, in.

δ^* boundary-layer displacement thickness for incompressible flow, $\delta\int_0^{1.0}\left(1 - \frac{u}{U}\right)d\left(\frac{y}{\delta}\right)$

θ boundary-layer momentum thickness for incompressible flow, $\delta\int_0^{1.0}\frac{u}{U}\left(1 - \frac{u}{U}\right)d\left(\frac{y}{\delta}\right)$

H boundary-layer shape parameter for incompressible flow, δ^*/θ

Diffuser performance parameters:

$\frac{\Delta\bar{h}}{q_{c_1}}$ total-pressure-loss coefficient

$\frac{\Delta p}{\Delta p_{ideal}}$ diffuser effectiveness

Subscripts:

0 reference conditions

1 diffuser-inlet conditions

6 diffuser-exit conditions

7 tailpipe-exit conditions

max maximum value

x longitudinal distance along length of diffuser

APPARATUS AND TESTS

General arrangement.- A schematic drawing of the apparatus used for this investigation is shown in figure 1. The test duct system consists of a 23° conical diffuser with a 2:1 ratio of exit to inlet area joined

to a 21-inch-diameter cylindrical approach tube approximately $4\frac{1}{2}$ inlet diameters in length. The junction between the approach tube and diffuser was formed as a circular arc of $5\frac{3}{16}$-inch radius, tangent to both the inlet cylinder and diffuser cone. A discharge tailpipe approximately $3\frac{1}{2}$ inlet diameters in length was attached to the diffuser exit. For all configurations, a 1-inch-wide roughness strip was permanently installed near the diffuser inlet to stabilize the flow. This strip is shown in figures 2 and 3.

Roughness particle size.- The cork particles of which the surface roughness was composed were the same size as those used for the investigation of reference 1. These particles will pass through a standard screen with 8 meshes to the inch but will be retained on a standard screen with 14 meshes to the inch. The average height of the particles used is approximately 0.10 inch. The data of reference 2 indicate that the average skin-friction coefficient for roughness made up of these particles is 0.0035 for a pipe. This value is about three times the value of the average skin-friction coefficient for the smooth-surface diffuser (ref. 3) over the range of Reynolds numbers investigated.

Description of configurations.- The cork particles were uniformly cemented about the interior surface of the diffuser in various extents of surface roughness. The leading edges of the roughness of the configurations are shown in figure 3(a) and the configurations are designated V, VI, VII, and VIII to conform with the designation system used in reference 1. The first series of pressure measurements was made for configuration V which had about 86 percent of the diffuser length roughened. Succeeding configurations VI, VII, and VIII had approximately 70, 54, and 32 percent of the diffuser length roughened, respectively. The 1-inch roughness strip near the inlet was included for all computations of percentages of diffuser length roughened. Incremental bands of cork were removed from the upstream edge after each series of pressure measurements was made so that the variation of the diffuser performance with percent of diffuser length roughened could be determined. It should be noted (fig. 3) that the extent of the smooth surface between the trailing edge of the inlet roughness strip and the leading edge of the main roughness region becomes larger with the removal of each incremental band of roughness. For each series of pressure measurements, the leading edge of the roughness was buffed and faired smoothly into the diffuser wall to a point about 2 inches downstream of the leading edge.

Instrumentation and inlet calibration.- A series of static-pressure orifices were installed along one generatrix of the diffuser and tailpipe to measure longitudinal static-pressure distributions. As is pointed out in reference 1, the static-pressure measurements obtained from orifices

located in the roughened area are believed to be accurate. At stations 1, 6, and 7 (fig. 1), wall static-pressure measurements were made at six equally distributed positions around the circumference. Pitot-static-pressure surveys also were made at longitudinal stations 2, 3, 4, and 5 between the diffuser inlet and exit for purposes of studying the boundary-layer development. The locations of these stations are indicated in figure 1.

The flow conditions at the diffuser inlet, station 1, were carefully explored and calibrated by making pitot-static-pressure surveys at three equidistant points around the circumference of the inlet. Typical velocity profiles measured at the diffuser inlet are shown in figure 4 for several values of inlet pressure ratio p_1/p_0. The results of the diffuser-inlet calibration are shown in figure 5 in which the inlet Mach number, the Reynolds number based on inlet diameter, the weight flow adjusted for standard stagnation conditions of 29.92 inches of mercury and 520° R, and a curve of p_1/h_0 are all plotted as functions of the inlet pressure ratio.

For all configurations, three pitot-static-pressure surveys were made simultaneously at three equally distributed positions in the transverse plane of station 6, for the purpose of checking flow symmetry.

Weight-flow check.- The weight flows were calculated for each configuration at both the diffuser exit and tailpipe exit. The results of these calculations are shown in figure 6 in which the standardized weight flow is plotted as a function of the inlet pressure ratio for all configurations at stations 1, 6, and 7. For all configurations the weight flows calculated from pitot-static-pressure measurements at the diffuser exit, given in figure 6(a), are slightly larger than the weight flows calculated from such measurements at the inlet, especially at the higher velocities. Discrepancies between inlet and exit weight flows were noted in references 1 and 4, and reference 5 provides a method for estimating the effect on the performance results of pressure measurements which lead to such weight-flow discrepancies. An estimation made with the use of the procedure of reference 5 indicated that for configurations VI and VII, for which the weight-flow discrepancies are greatest at the diffuser exit, the calculated values of diffuser total-pressure-loss coefficient, discussed in the section entitled "Results and Discussion," are probably of the order of 5 percent lower than the true mean values.

The measured weight-flow values for configurations V and VIII at the diffuser exit, station 6, and for all the configurations at the tailpipe exit, station 7, indicate that any attempted correction similar to that of reference 5 for these cases would amount to less than the data scatter. No total-pressure-loss-coefficient corrections were made, therefore, for any of the data presented.

METHODS AND ANALYSIS

Because a reference total-pressure tube installed in a small plenum chamber of the present apparatus would produce disturbances in the inlet flow, the static pressure p_0 was used as the reference pressure. In reference 1, the plenum chamber was larger; therefore, a total-pressure tube was installed and the inlet total pressure h_0 was used as the reference pressure. Thus, all comparisons between the data for the present investigation and those reported in reference 1 were made by using the calibration curve of figure 5(d) in which p_1/h_0 is plotted against p_1/p_0.

Calculation of pressure differences.- The volume-weighted mean loss in total pressure from the reference station 0 to the station under consideration was computed in the following manner:

$$p_0 - \bar{h}_x = \frac{2\pi \int_0^R u\left(p_0 - h_x\right) r \, dr}{2\pi \int_0^R ur \, dr} \tag{1}$$

The mean loss in total pressure was computed for both the diffuser and diffuser plus tailpipe by using the following relations:

For the diffuser:

$$\Delta\bar{h}_{1,6} = \left(p_0 - \bar{h}_6\right) - \left(p_0 - \bar{h}_1\right) \tag{2}$$

For the diffuser plus tailpipe:

$$\Delta\bar{h}_{1,7} = \left(p_0 - \bar{h}_7\right) - \left(p_0 - \bar{h}_1\right) \tag{3}$$

The rise in static pressure was computed as the difference between the arithmetic mean of the six wall static-pressure measurements at station 1 and the arithmetic mean of the wall static-pressure measurements at station 6 or 7. The theoretical gain in static pressure was computed by assuming frictionless, incompressible, one-dimensional flow with the same entering mass flow and geometric area.

Diffuser performance parameters.- In order to provide a basis for comparing the results of the present investigation with those of reference 1, the same performance parameters as presented therein are used in the present analysis. The coefficients are given as follows:

(1) The total-pressure-loss coefficient, defined as the loss in mean total pressure divided by the inlet impact pressure, $\Delta\bar{h}/q_{c_1}$

(2) The diffuser effectiveness, defined as the actual gain in static pressure divided by the gain in static pressure possible with frictionless flow, $\Delta p/\Delta p_{ideal}$

RESULTS AND DISCUSSION

In the present investigation the same inlet-boundary-layer thickness existed as in that of reference 1. This inlet-boundary-layer thickness was of the order of 5 percent of the inlet diameter and corresponds to the thicker inlet-boundary-layer condition of reference 3. All comparisons between the data presented herein and those of reference 1 or 3 are made for this inlet-boundary-layer condition.

Flow in Roughened Diffuser

In contrast to the flow in the smooth-surface diffuser (ref. 3) which periodically shifted position and lacked reproducibility, the flow in the roughened diffuser was steady and reproducible. Although flow separation was found at the diffuser exit for some configurations, this condition was not characterized by violent oscillations of the fluid in the manometer tubes. Furthermore, it was found that the data were readily repeatable for the cases in which boundary-layer separation appeared.

As pointed out in reference 3, difficulty in making pressure surveys at the diffuser exit made it impossible in that investigation to present values of the total-pressure-loss coefficient at that point. In both the present investigation and that of reference 1, however, the steady flow at station 6 made it possible to make detailed pressure surveys at that point and values of $\Delta\bar{h}/q_{c_1}$ are presented at station 6 for all configurations. The diffuser effectiveness is the only performance parameter for which an exact comparison can be made at the diffuser exit (station 6) between the smooth-surface-diffuser results of reference 3 and the present study.

Boundary-Layer and Diffuser Performance Results

For all configurations, the velocity profiles computed from pitot-static-pressure surveys made at seven stations along the wall of the diffuser and tailpipe on a single generatrix are shown in figures 7 to 10 for three approximately constant values of p_1/p_0. Included with each of the profiles shown in figures 7 to 10 are the values of the boundary-layer displacement and momentum thicknesses and the boundary-layer shape parameter. Velocity profiles at three equidistant points on the circumference in the plane of station 6 are shown in figure 11 for an approximately constant inlet pressure ratio of 0.94. The boundary-layer parameters δ^*, θ, and H, calculated from test data, are plotted against the inlet pressure ratio in figures 12 to 16, for each of the roughness configurations. Values of δ^*, θ, and H selected from the faired curves of figures 12 to 16 at an inlet pressure ratio of 0.95 are plotted in figure 17 to show the development of the boundary layer along the length of the diffuser for each of the roughness configurations.

Figure 18 shows a comparison between the static-pressure distributions for each of the roughness configurations at an approximately constant inlet pressure ratio of 0.95. The variation of the diffuser effectiveness and total-pressure-loss coefficient with inlet pressure ratio are shown in figures 19 and 20, respectively, for all four of the configurations investigated. A comparison between the diffuser-exit (station 6) velocity profiles for all configurations, including configuration I of reference 1, is shown in figure 21. Figure 22 presents a résumé and comparison between the performance results for the present investigation and those of reference 1.

Diffuser boundary-layer velocity profiles.- The results for the boundary-layer velocity profile along the diffuser and at the tailpipe exit are shown in figures 7 to 10 and indicate that, for each of the roughness configurations, flow separation occurred or appeared imminent at the downstream measuring stations 5 and 6. The data shown in figure 7 indicate that configuration VIII (32 percent of diffuser length roughened) produced separated flow from about x equals 14.5 inches to x equals 24.6 inches (stations 4, 5, and 6) at all velocities. The profiles shown for configurations VII, VI, and V (54, 70, and 86 percent of diffuser length roughened, respectively) indicate different degrees of imminent separation at stations 5 and 6. (See figs. 8 to 10.) These results suggest the probability of asymmetrical flow conditions in the downstream regions of the diffuser for all configurations and caution should therefore be exercised in interpreting the results in terms of the standard boundary-layer parameters.

An indication of the asymmetry of the diffuser flow may be obtained from the measurements made along three equally spaced radii at the

diffuser exit, station 6. These measurements are presented in figure 11 in terms of boundary-layer velocity distributions for each of the roughness configurations investigated. For configuration VIII (32 percent of diffuser length roughened), large variations in profiles were obtained with separated flow being indicated in one position, as noted in figure 7, and attached flow being indicated in the other two positions. In general, as the extent of roughness was increased, the degree of asymmetry tended to decrease, with configuration V (86 percent of diffuser length roughened) exhibiting quite symmetrical flow. The flow asymmetries obtained preclude detailed interpretation of the boundary-layer measurements along any single diffuser generatrix according to boundary-layer theory for symmetrical flow. However, the general trends indicated by the curves shown in figure 17 are considered realistic.

Boundary-layer displacement thickness.- The curves shown in figure 17(a) indicate that the variation of the boundary-layer displacement thickness along the length of the diffuser is approximately the same for all configurations within about ±10 percent. It can be seen that the values of δ^* for configuration VIII (32 percent of diffuser length roughened) at stations 4, 5, and 6 (x = 14.5, 19.8, and 24.6 inches) are somewhat higher than the values of δ^* for the other configurations. This result is probably due to the separated flow indicated in figure 7 at these stations.

Since the value of δ^* at any point along the wall of the diffuser determines the effective area of the duct at that point, it would be expected that the axial static-pressure distribution would be approximately the same for all configurations. This conclusion is supported by the results shown in figure 18, in which the ratio of static pressure at points along the length of the diffuser to the static pressure at the diffuser inlet is plotted against distance along the longitudinal axis for approximately the same inlet pressure ratio for all configurations. The deviation of the data from a single curve results in a difference of about 10 percent in the pressure recovery for the most divergent case.

Since the differences in static pressure due to changes in roughness length are small, and since all configurations produced approximately the same δ^* variation, it can be concluded that changes in roughness length would not produce significant changes in the overall static-pressure recovery. This conclusion is substantiated by the curves of figure 22(a) which show the variation of diffuser effectiveness with percent of diffuser length roughened. Examination of these curves indicates that, although the diffuser effectiveness diminishes slightly as the extent of roughness is increased, the differences are very small.

Boundary-layer momentum thickness.- The variation of the boundary-layer momentum thickness along the length of the diffuser is shown in figure 17(b) for all configurations. For configurations V, VI, and VII

(86, 70, and 54 percent of diffuser length roughened, respectively), the momentum-thickness variation was very similar and differences between these curves are not considered large enough to be regarded as significant. The values of θ for configuration VIII (32 percent of diffuser length roughened) are considerably lower than those for the other roughness configurations; however, these values of θ cannot be regarded as representative values occurring at other circumferential locations in the diffuser because of the flow asymmetry resulting from the separation in the downstream regions.

Boundary-layer shape parameter.- The curves of boundary-layer shape parameter shown in figure 17(c) indicate that for configuration V the rate of growth of H is essentially constant over the diffuser length. For configurations VI, VII, and VIII, the slopes of the H curves have been caused to reverse in sense near the diffuser exit.

Diffuser-exit velocity profiles.- Although the values of H at the diffuser exit vary from about 3.0 to 3.5 for the different configurations (fig. 17(c)), it is not apparent whether these values represent large differences in the velocity-profile shapes, unless the physical shapes of the velocity profiles are compared. In order to determine whether significant differences exist between the diffuser-exit velocity profiles for all configurations, figure 21 compares station 6 velocity profiles at a constant inlet pressure ratio of 0.95. Significant differences between velocity profiles for all configurations are detectable.

A comparison between the data shown in figures 7 to 10 and the data of figure 21 indicates some differences between the two sets of data. These differences occur because the profiles of figure 21 represent an average of the three radial surveys, shown in figure 11, whereas the data shown in figures 7 to 10 correspond to radial surveys at one circumferential location.

In deciding which of the configurations produced the best overall performance, all aspects being considered, one would have to choose on the basis of the values of the total-pressure-loss coefficient and the exit-velocity distribution since the differences in static-pressure recovery were not significant. The configurations with 32 and 54 percent of the diffuser length roughened produced the highest total-pressure-loss coefficients as well as flow asymmetries at the diffuser exit; thus, these configurations are undesirable. Figure 22(b) indicates that the total-pressure-loss coefficient for the configuration with 86 percent of the diffuser length roughened is about 10 percent lower than that for the configuration with 70 percent of the diffuser length roughened and figure 11(d) indicates that it had the best flow symmetry characteristics. Configuration V, therefore, appears to be the best from an overall performance standpoint in the present investigation.

Comparison Between Present Results and Those of Reference 1

The results of the present investigation can be shown to be in accord with those of reference 1. To illustrate this fact, figure 22 shows the variation of $\Delta p/\Delta p_{ideal}$ and $\Delta\bar{h}/q_{c_1}$ with percent of diffuser length roughened for both the diffuser and the tailpipe exits, stations 6 and 7, at a constant inlet pressure ratio of 0.95. A comparison between the results of the present investigation and the results of reference 1 is also shown in this figure. Figure 22(a) indicates that the static-pressure-recovery results for the present investigation and for the investigation of reference 1 are, in general, very much the same. Consequently, the displacement thicknesses for the diffuser-exit velocity profiles are very similar in magnitude for both investigations. This fact can be seen by comparing values of δ^* for the diffuser-exit velocity profiles given in reference 1 and the range of values of δ^* shown in figure 17(a) at station 6 ($x = 24.6$ inches). Figure 22(b) shows that, although the maximum values of the total-pressure-loss coefficient occur at approximately the same condition (45 percent of the diffuser length roughened), the maximum values of $\Delta\bar{h}/q_{c_1}$ at both measuring stations are somewhat less for the present investigation than those found in the results of reference 1. This observation is readily explainable when it is considered that, for the investigation of reference 1, the roughness extended from a point near the inlet in a downstream direction, whereas the present results are for the case of roughness extending from the diffuser exit in an upstream direction. The exit-velocity profile data of reference 1 indicate further that the 97-percent-roughness configuration produced the best velocity distribution (see fig. 21). The 97-percent-roughness case also produced the smallest total-pressure-loss coefficients; values for the tailpipe exit and diffuser exit were lower than that for the tailpipe exit of the completely smooth surface diffuser by approximately 8 and 21 percent, respectively.

CONCLUSIONS

From the investigation of NACA RM L51K09 and the present investigation regarding the effect of surface roughness on the performance of a 23° conical diffuser with a 2:1 ratio of exit to inlet area and a constant-area tailpipe $3\frac{1}{2}$ inlet diameters in length, and with an inlet-boundary-layer thickness of approximately 5 percent of the inlet diameter, the following conclusions are drawn:

1. The results of the present investigation and those of NACA RM L51K09 indicate that the flow in the roughened diffuser (including that for the inlet roughness strip only), even though asymmetrical for some configurations, was steady and reproducible for all conditions, including those with separated flow.

2. The 97-percent-roughness case produced the smallest total-pressure-loss coefficients; values for the tailpipe exit and diffuser exit were lower than that for the tailpipe exit of the completely smooth surface diffuser by 8 and 21 percent, respectively. The experimental results indicated that maximum values of total-pressure-loss coefficient at both the diffuser and tailpipe exits were obtained for about 45 percent of the diffuser length roughened, without regard to whether the roughness was placed upstream or downstream, with the inlet roughness strip in place.

3. The results of the present investigation and those of NACA RM L51K09 indicated a trend toward reduction of asymmetry with increasing extent of surface roughness.

4. The static-pressure recovery at the diffuser exit diminished slightly as the extent of the roughness was increased from the smooth condition to the condition in which 97 percent of the diffuser length was roughened, whereas the diminution of the static-pressure recovery at the tailpipe exit was barely detectable over the range of roughness configurations investigated.

Langley Aeronautical Laboratory,
National Advisory Committee for Aeronautics,
Langley Field, Va., October 30, 1953.

REFERENCES

1. Persh, Jerome: The Effect of Surface Roughness on the Performance of a 23° Conical Diffuser at Subsonic Mach Numbers. NACA RM L51K09, 1952.

2. Nikuradse, J.: Laws of Flow in Rough Pipes. NACA TM 1292, 1950.

3. Persh, Jerome: The Effect of the Inlet Mach Number and Inlet-Boundary-Layer Thickness on the Performance of a 23° Conical-Diffuser - Tail-Pipe Combination. NACA RM L9K10, 1950.

4. Persh, Jerome, and Bailey, Bruce M.: Effect of Various Arrangements of Triangular Ledges on the Performance of a 23° Conical Diffuser at Subsonic Mach Numbers. NACA TN 3123, 1954.

5. Persh, Jerome, and Bailey, Bruce M.: A Method for Estimating the Effect of Turbulent Velocity Fluctuations in the Boundary Layer on Diffuser Total-Pressure-Loss Measurements. NACA TN 3124, 1954.

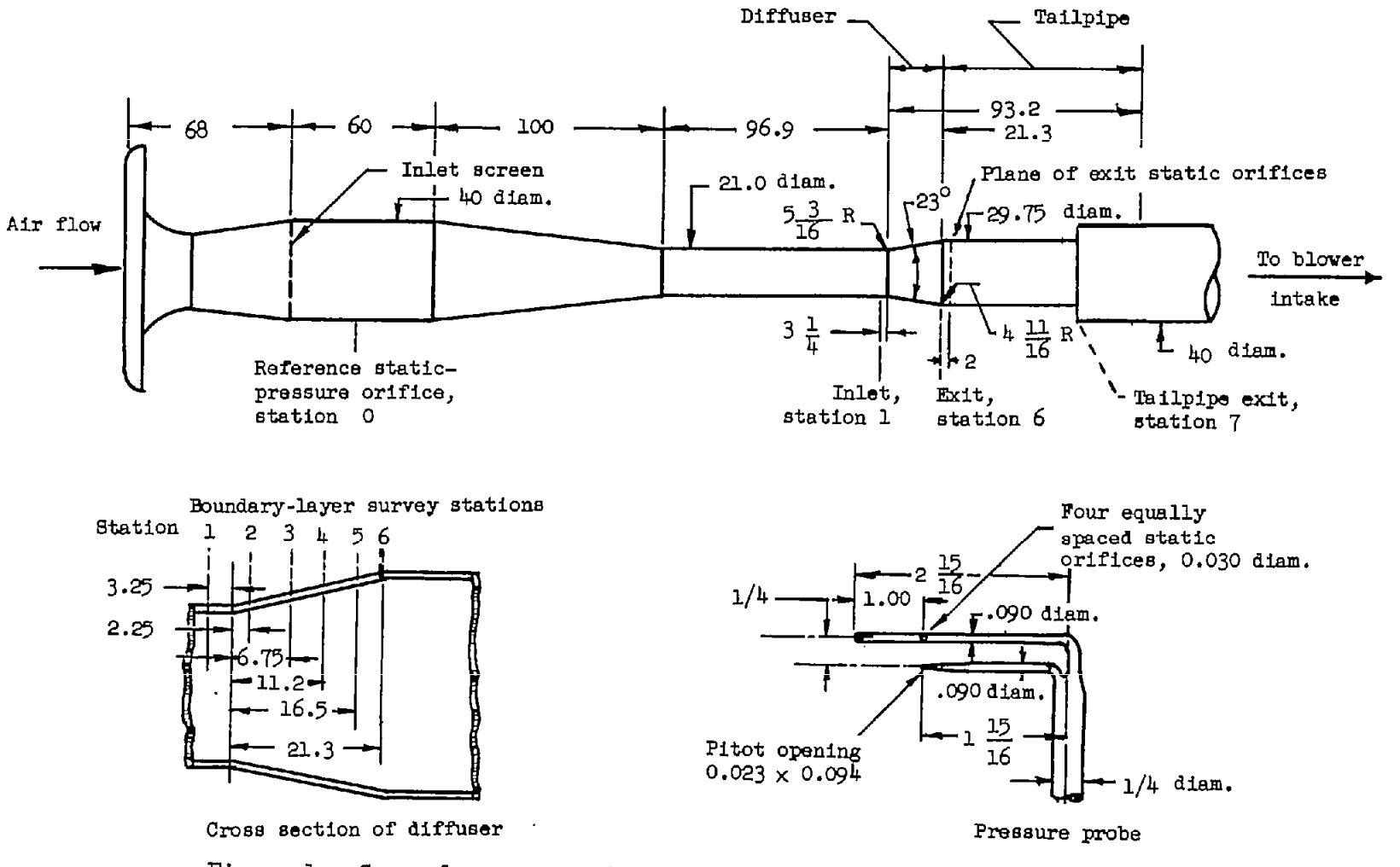

Figure 1.- General arrangement of test apparatus and instrumentation.
All dimensions are in inches.

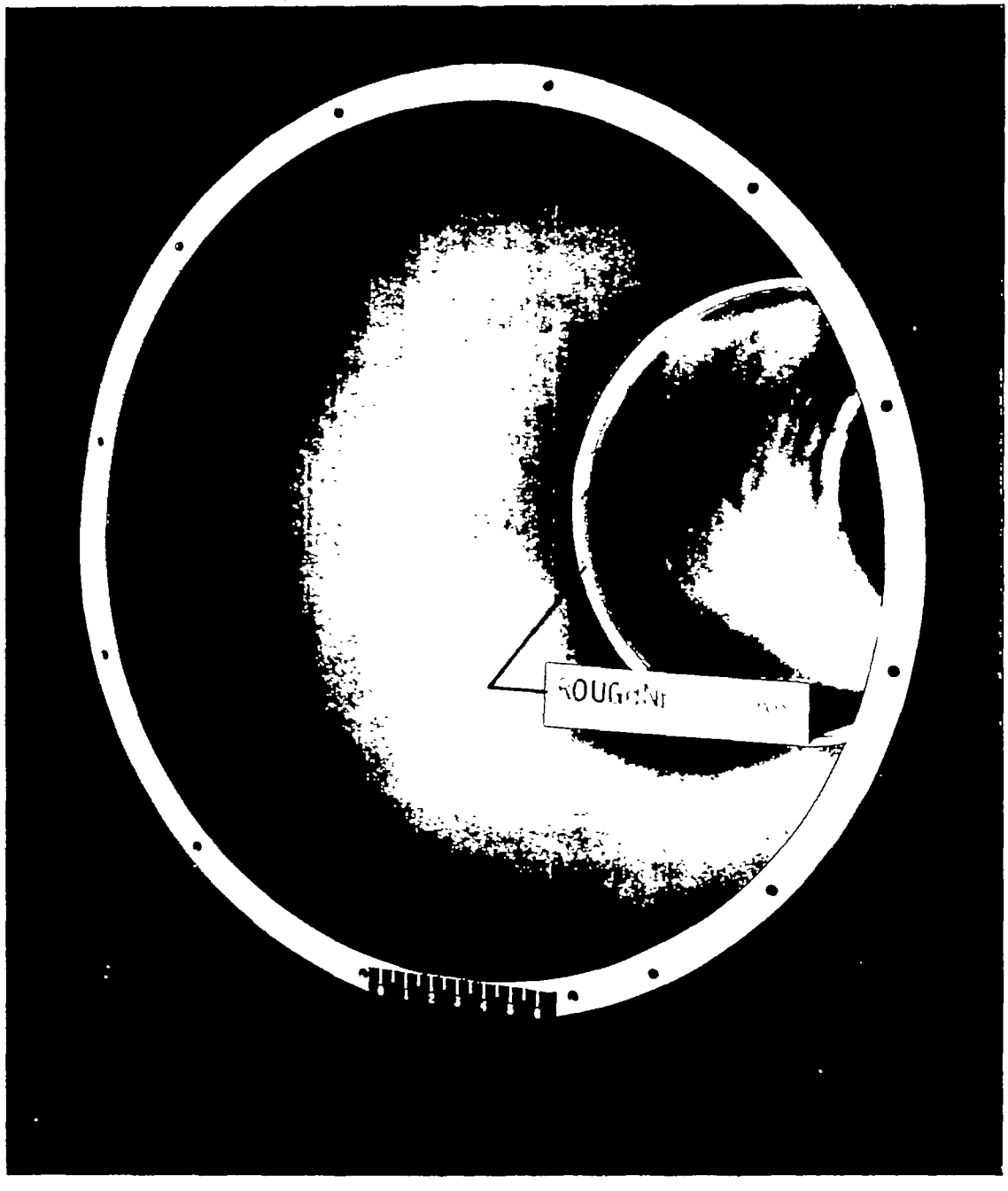

L-71847.1

Figure 2.- Three-quarter view of diffuser, looking upstream, showing inlet roughness strip in place.

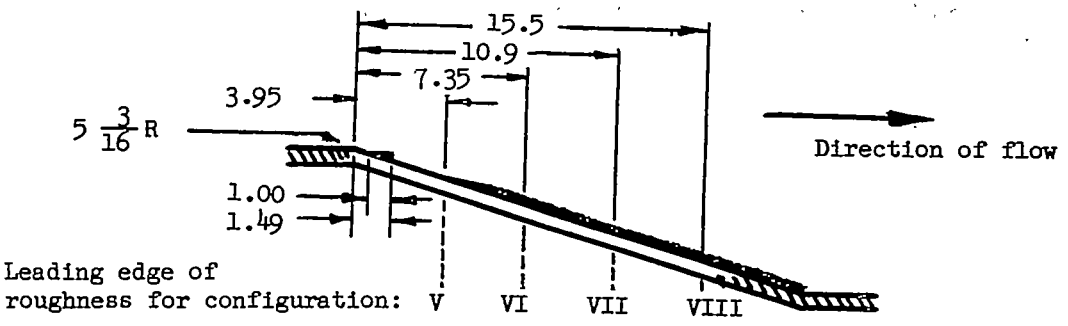

(a) Cross section of diffuser wall showing various surface-roughness dimensions relative to inlet.

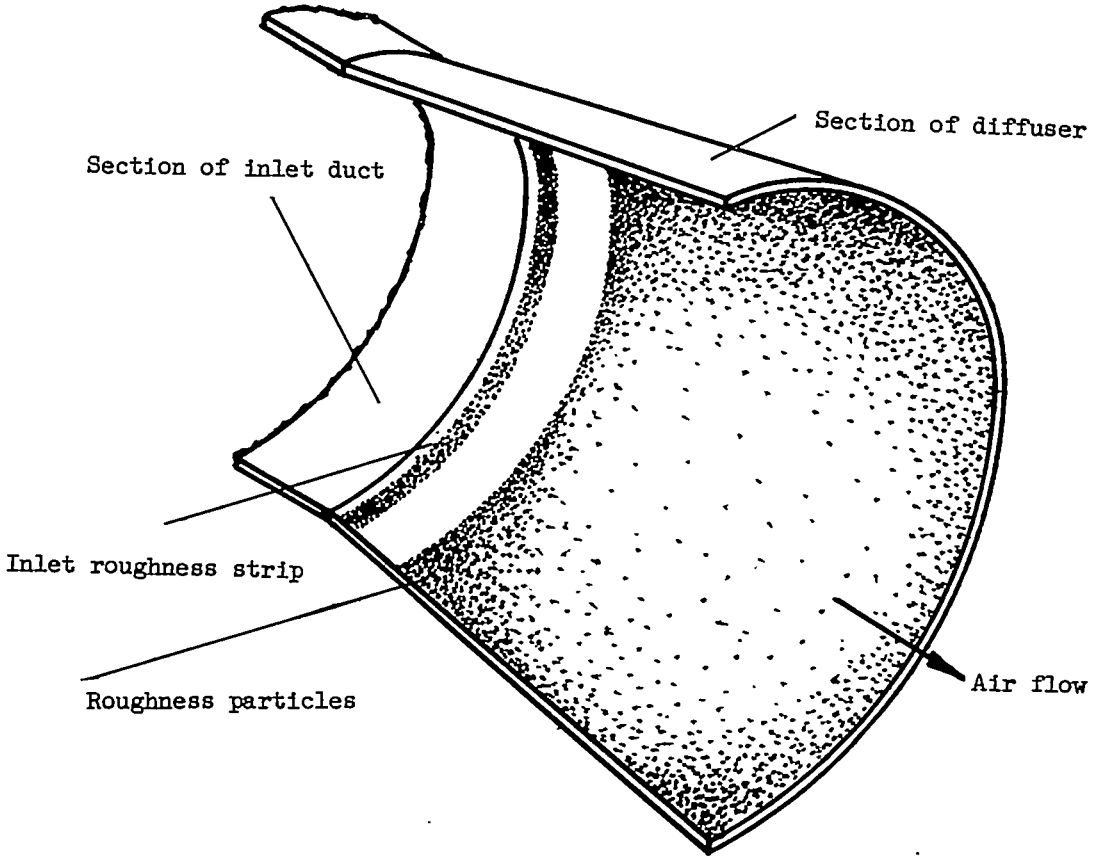

(b) Isometric view of cross section of diffuser with extent of roughness approximately representative of configuration V (86 percent of diffuser length roughened).

Figure 3.- Details of diffuser surface roughness. All dimensions are in inches.

$\frac{p_1}{p_0}$	δ*, in.	θ, in.	H
0.9880	0.188	0.135	1.390
.9792	.175	.133	1.320
.9600	.163	.128	1.275
.9100	.144	.119	1.200

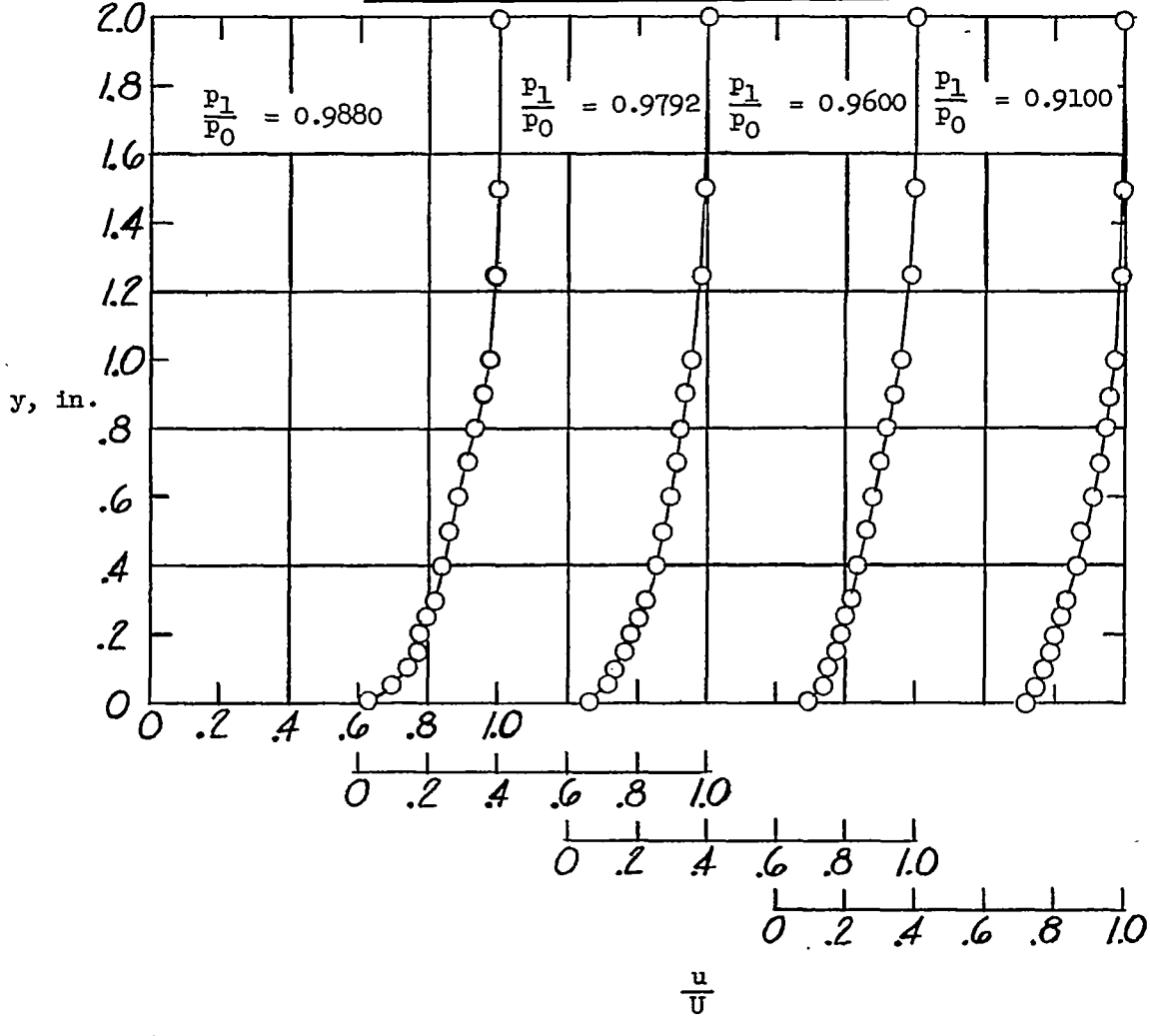

Figure 4.- Typical inlet velocity profiles at several values of inlet pressure ratio.

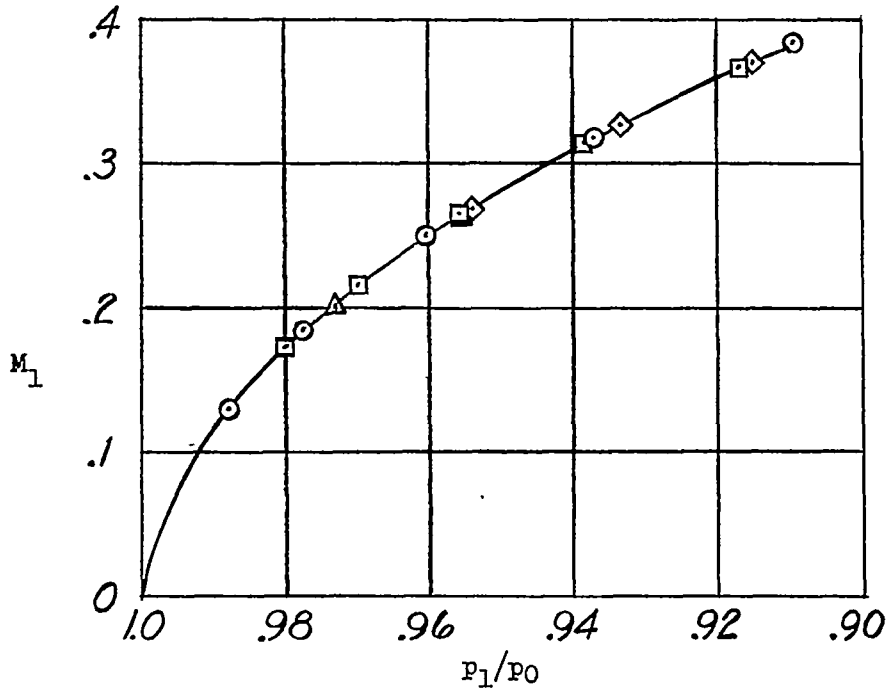

(a) Mach number.

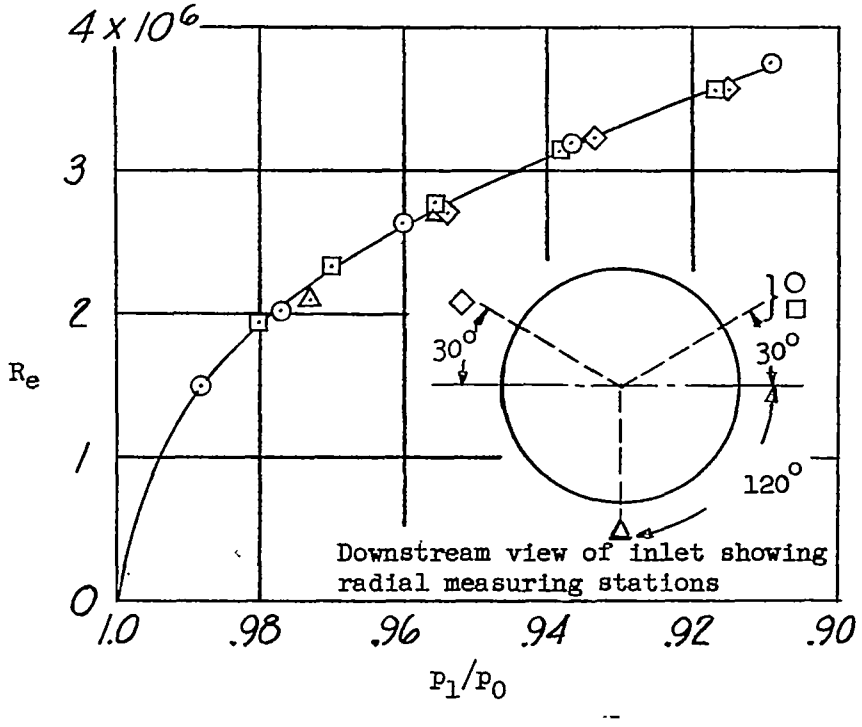

(b) Reynolds number.

Figure 5.- Variation of inlet conditions with inlet pressure ratio.

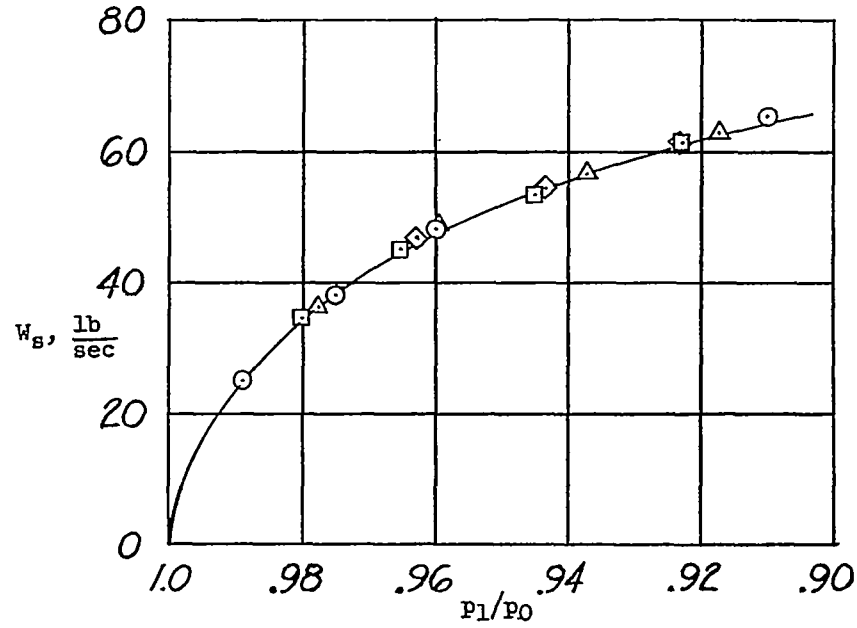

(c) Weight flow.

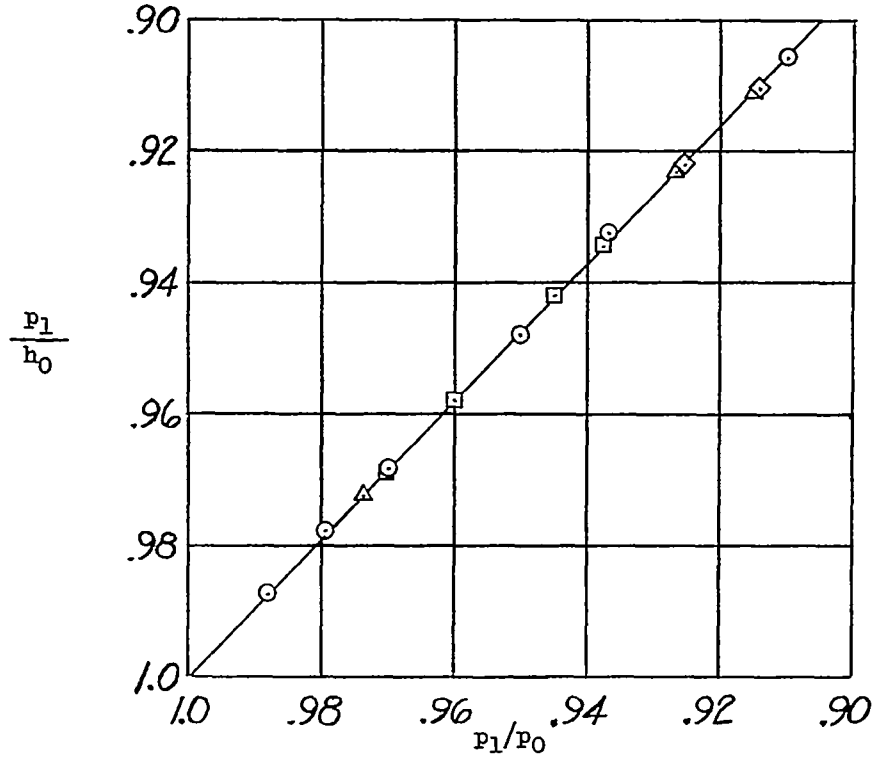

(d) Ratio of inlet static pressure to upstream total pressure.

Figure 5.- Concluded.

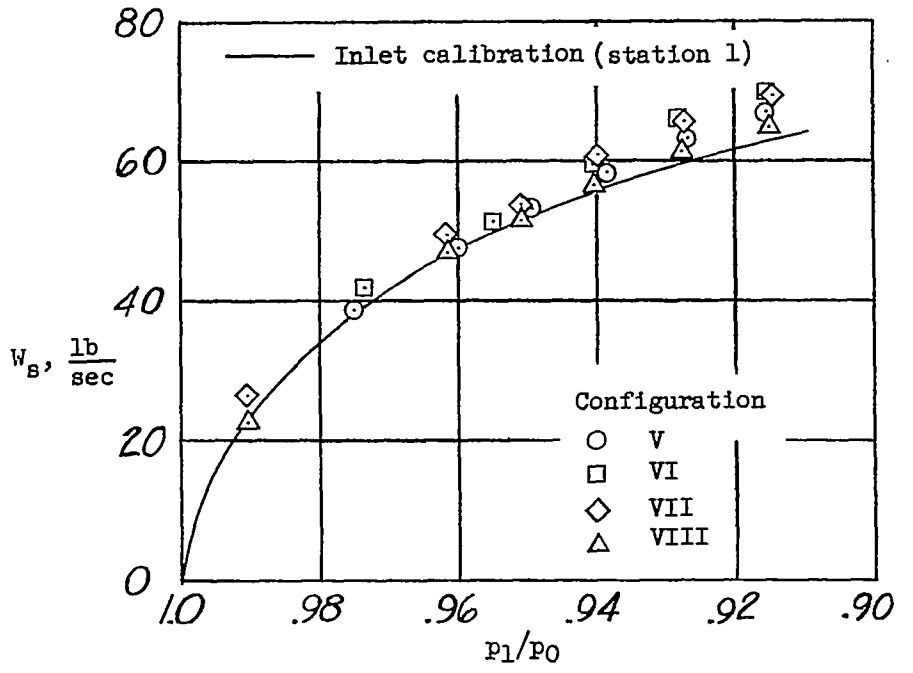

(a) From diffuser-exit measurements (station 6).

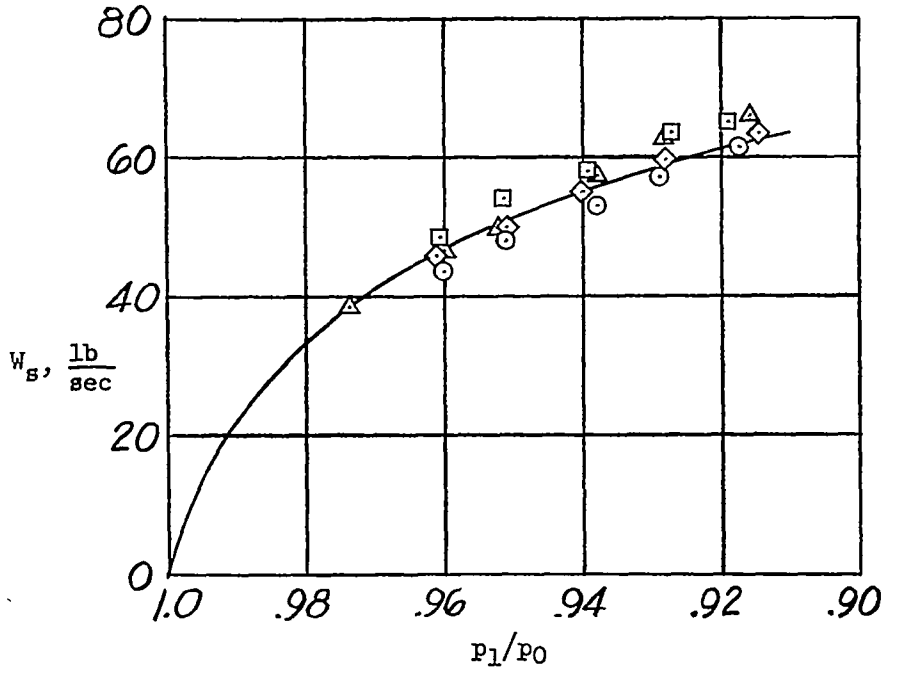

(b) From tailpipe-exit measurements (station 7).

Figure 6.- Weight-flow variation with p_1/p_0 from measurements at diffuser and tailpipe exits.

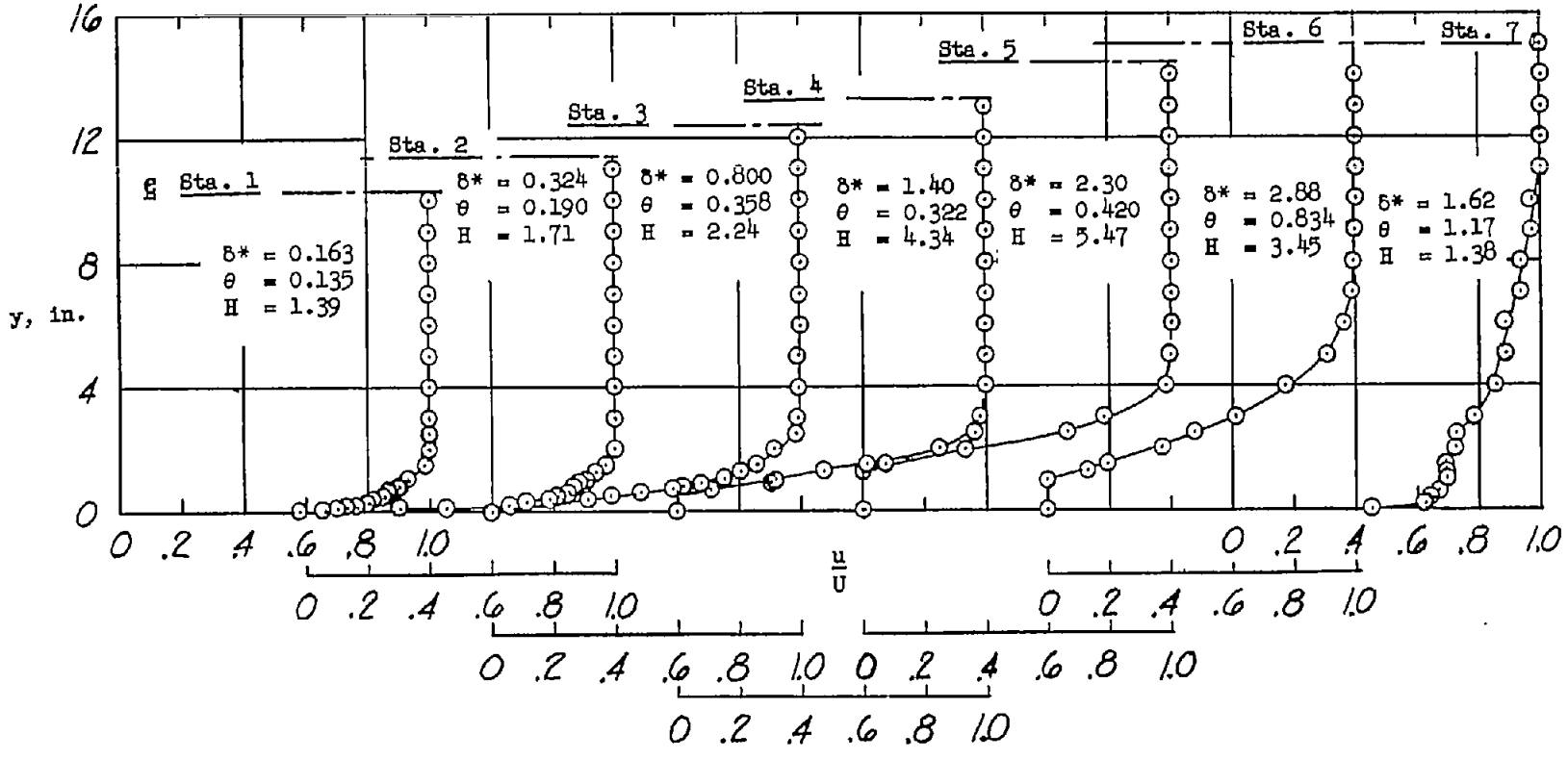

(a) $\frac{p_1}{p_0} \approx 0.96$.

Figure 7.- Boundary-layer velocity profiles along diffuser and at tailpipe exit for 32 percent of diffuser length roughened (configuration VIII).

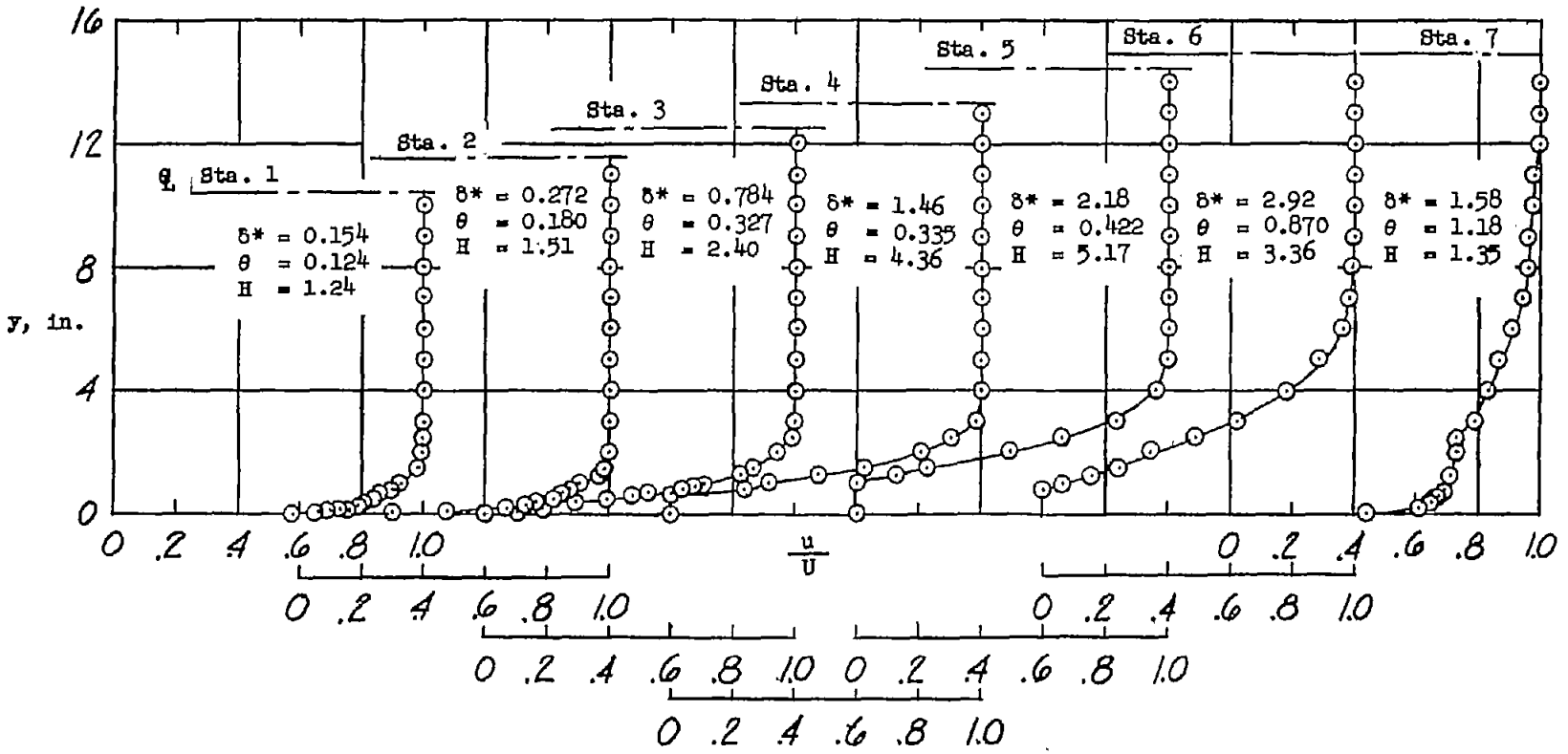

(b) $\frac{p_1}{p_0} \approx 0.94$.

Figure 7.- Continued.

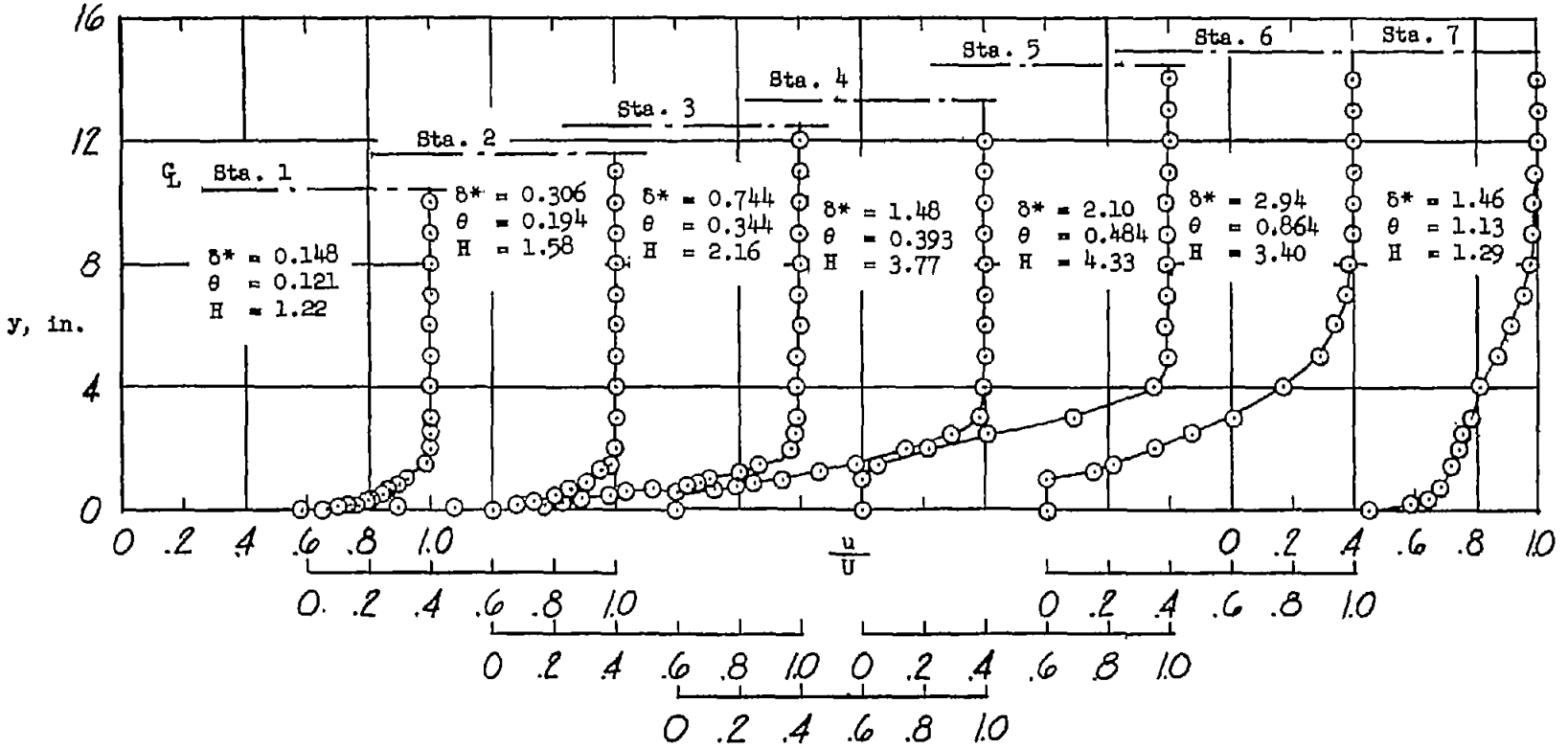

(c) $\frac{p_1}{p_0} \approx 0.915$.

Figure 7.- Concluded.

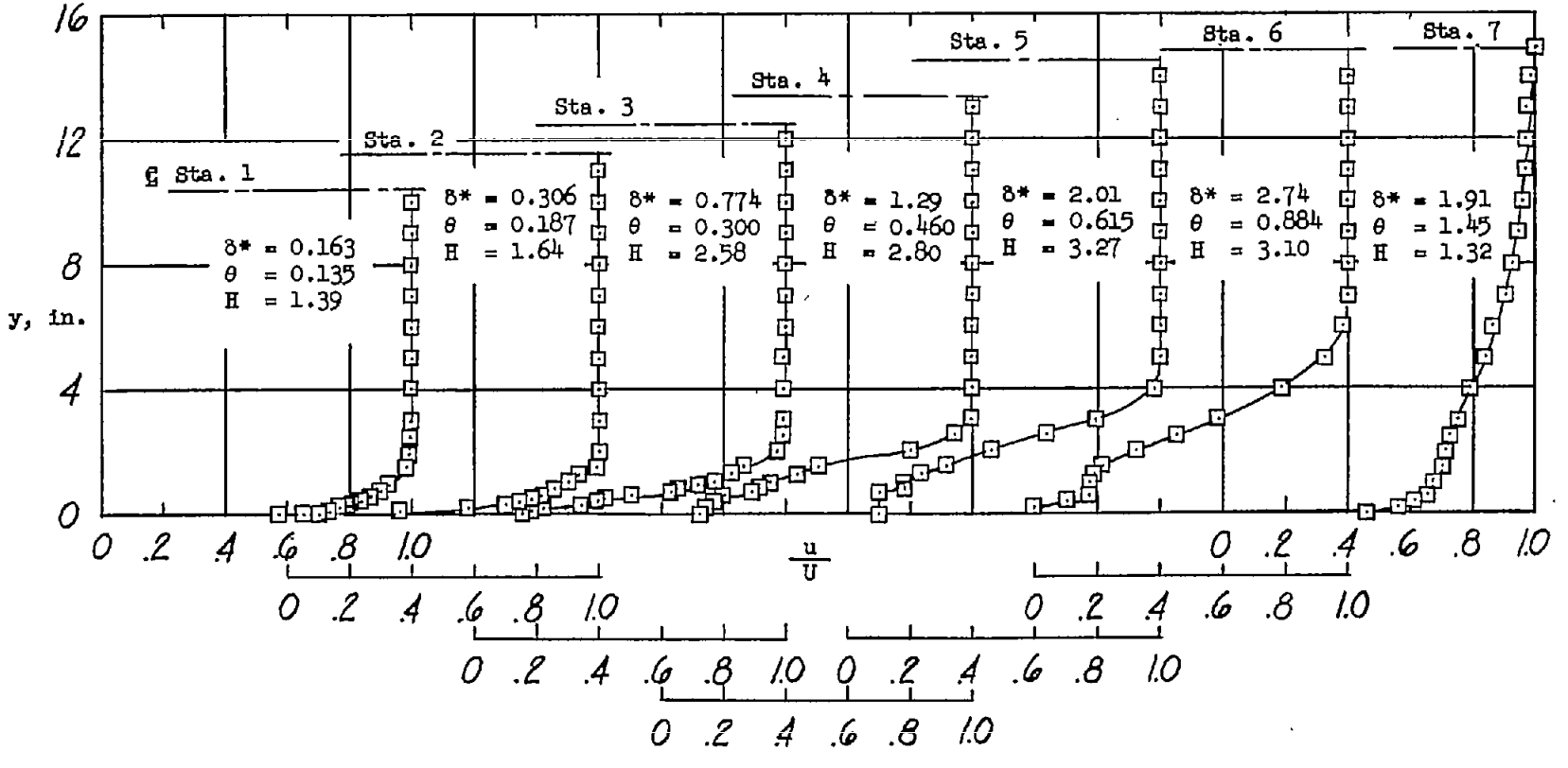

(a) $\frac{p_1}{p_0} \approx 0.96$.

Figure 8.- Boundary-layer velocity profiles along diffuser and at tailpipe exit for 54 percent of diffuser length roughened (configuration VII).

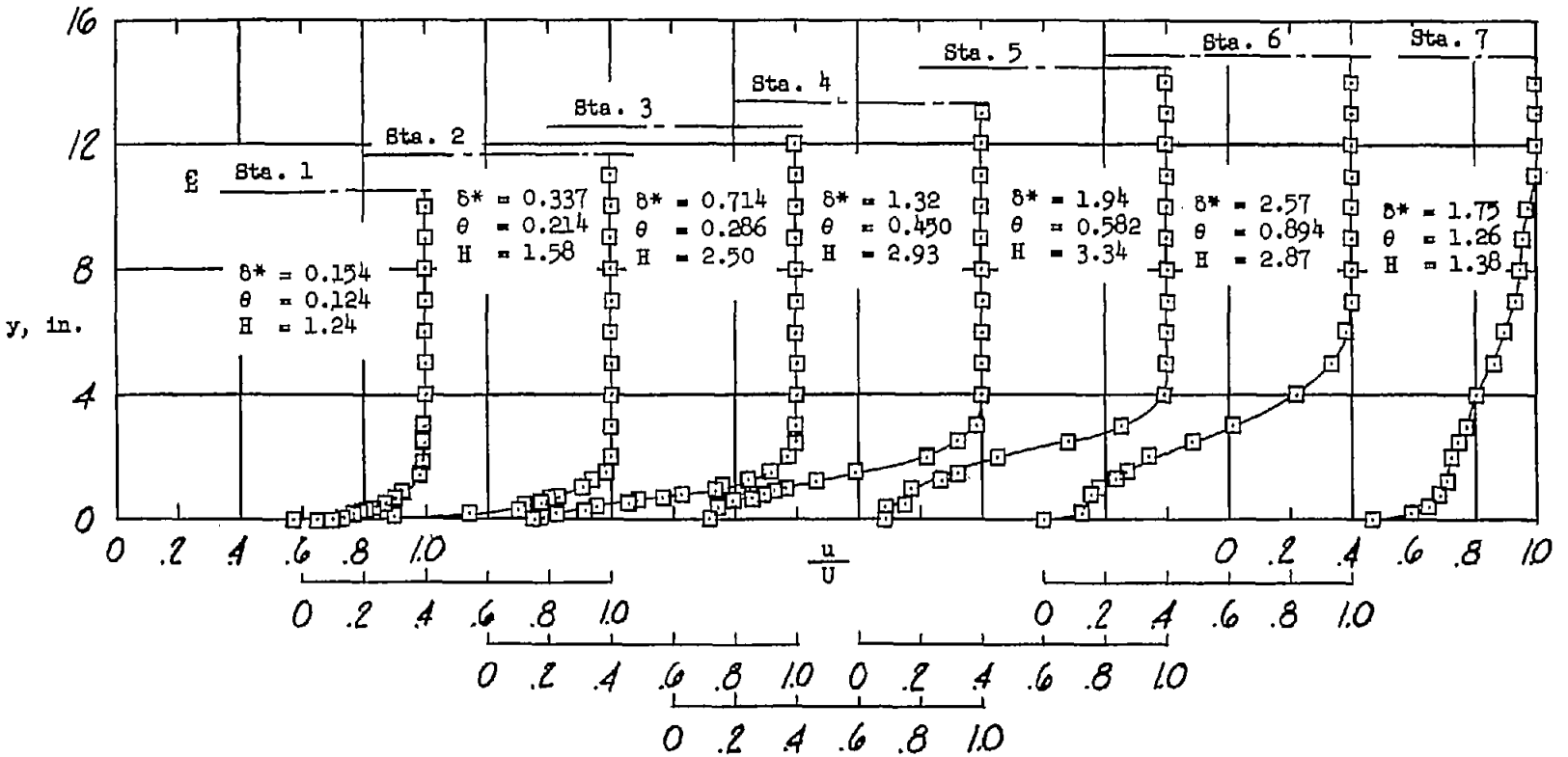

(b) $\frac{p_1}{p_0} \approx 0.94$.

Figure 8.- Continued.

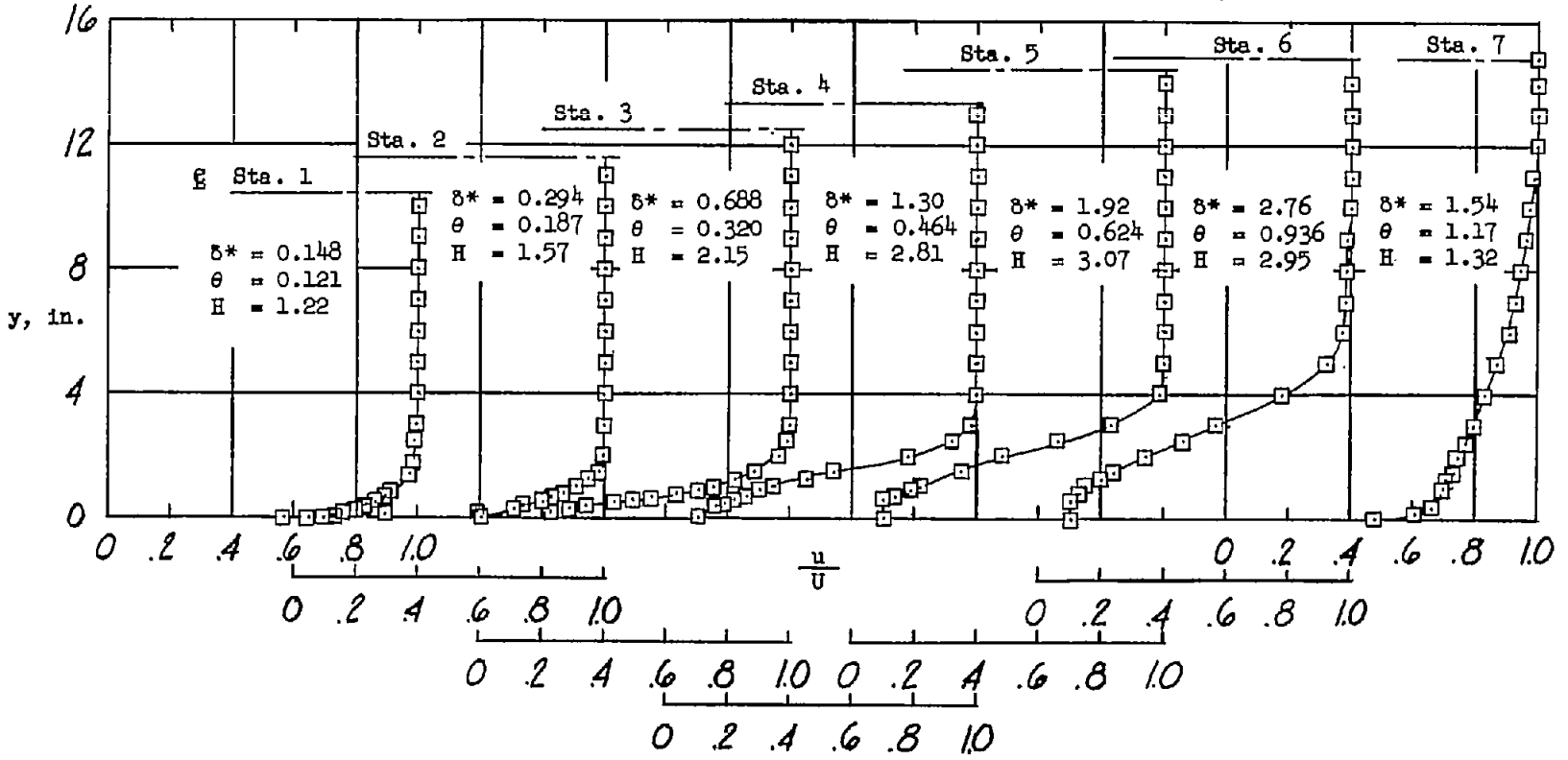

(c) $\frac{p_1}{p_0} \approx 0.915$.

Figure 8.- Concluded.

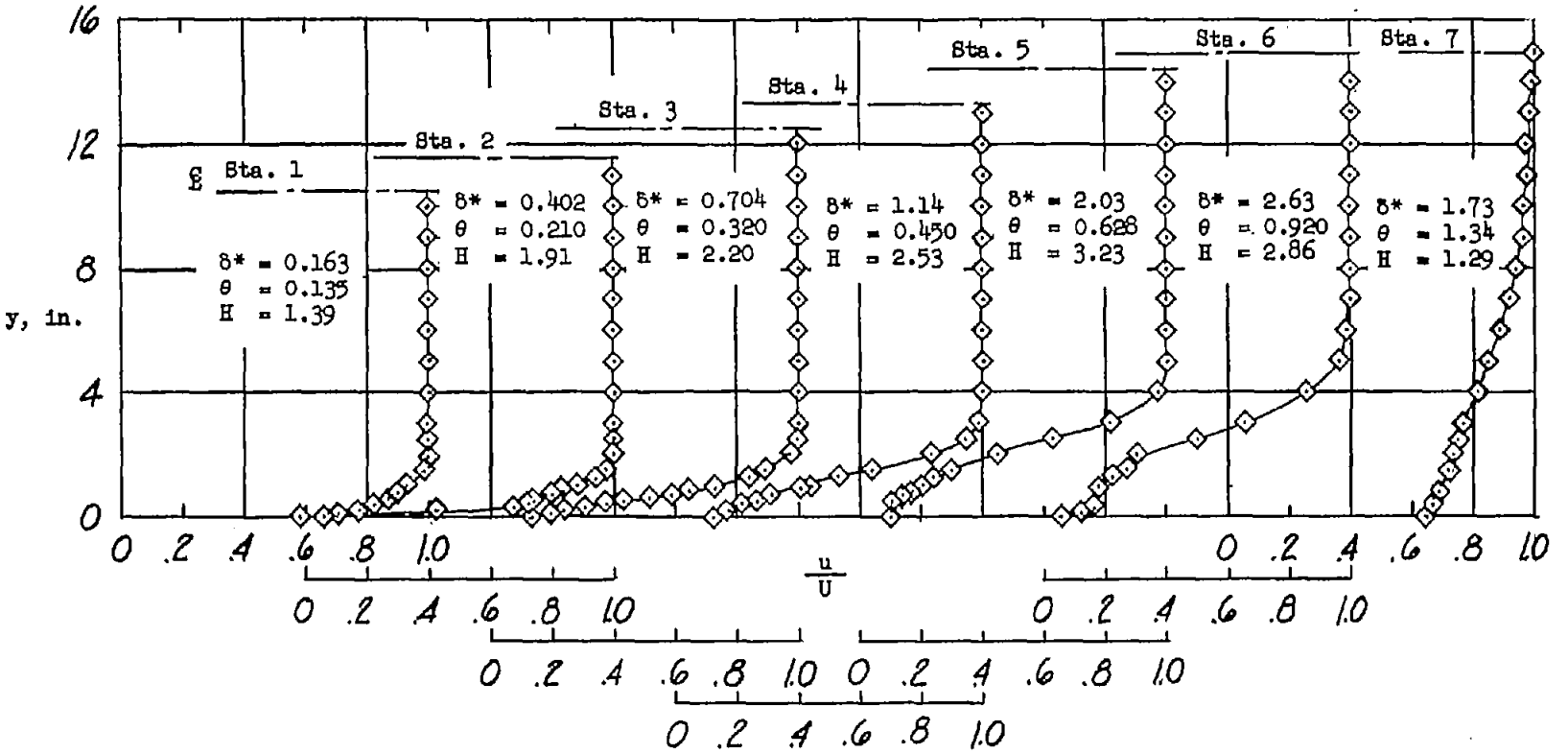

(a) $\frac{p_1}{p_0} \approx 0.96$.

Figure 9.- Boundary-layer velocity profiles along diffuser and at tailpipe exit for 70 percent of diffuser length roughened (configuration VI).

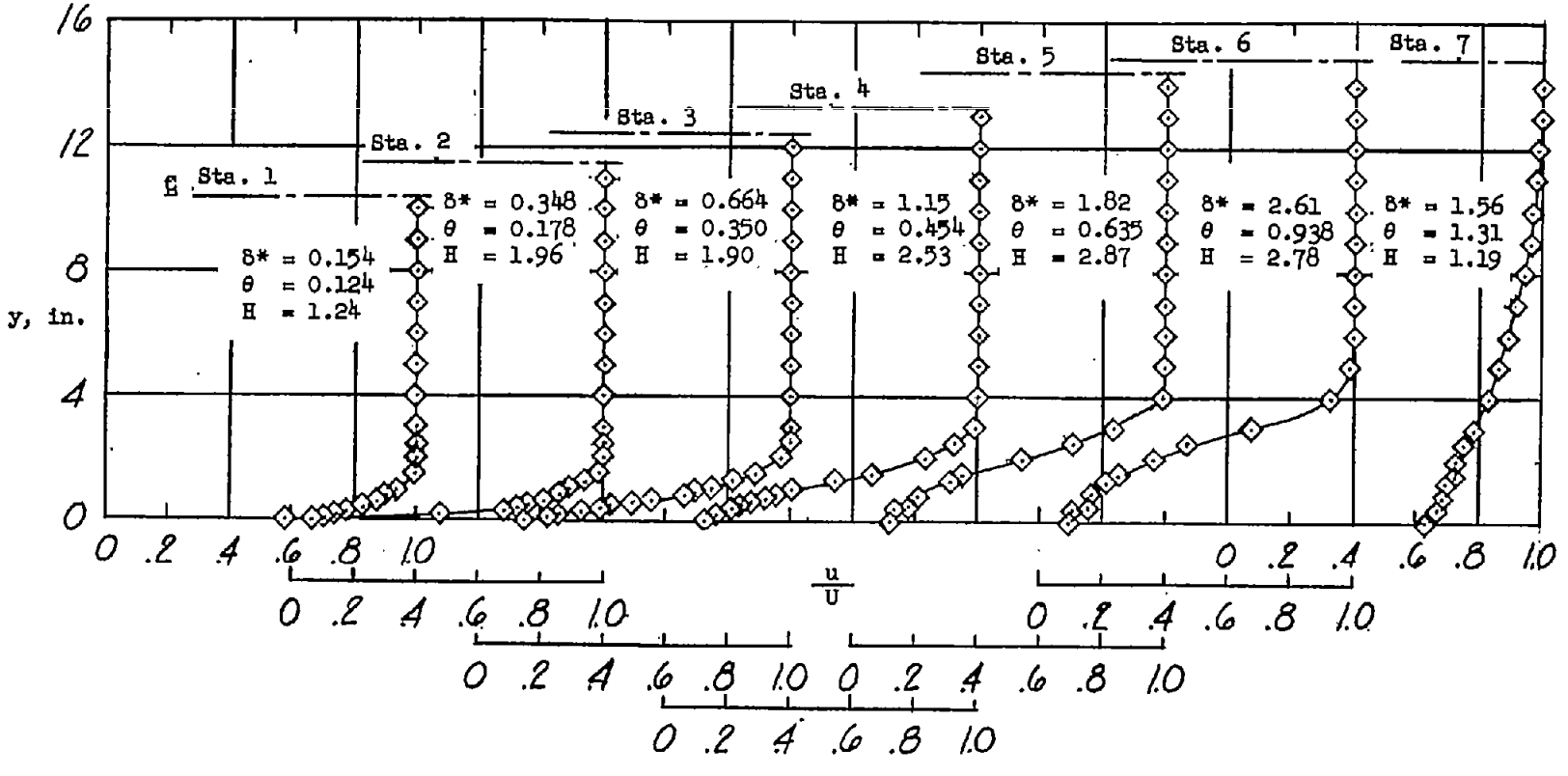

(b) $\frac{p_1}{p_0} \approx 0.94$.

Figure 9.- Continued.

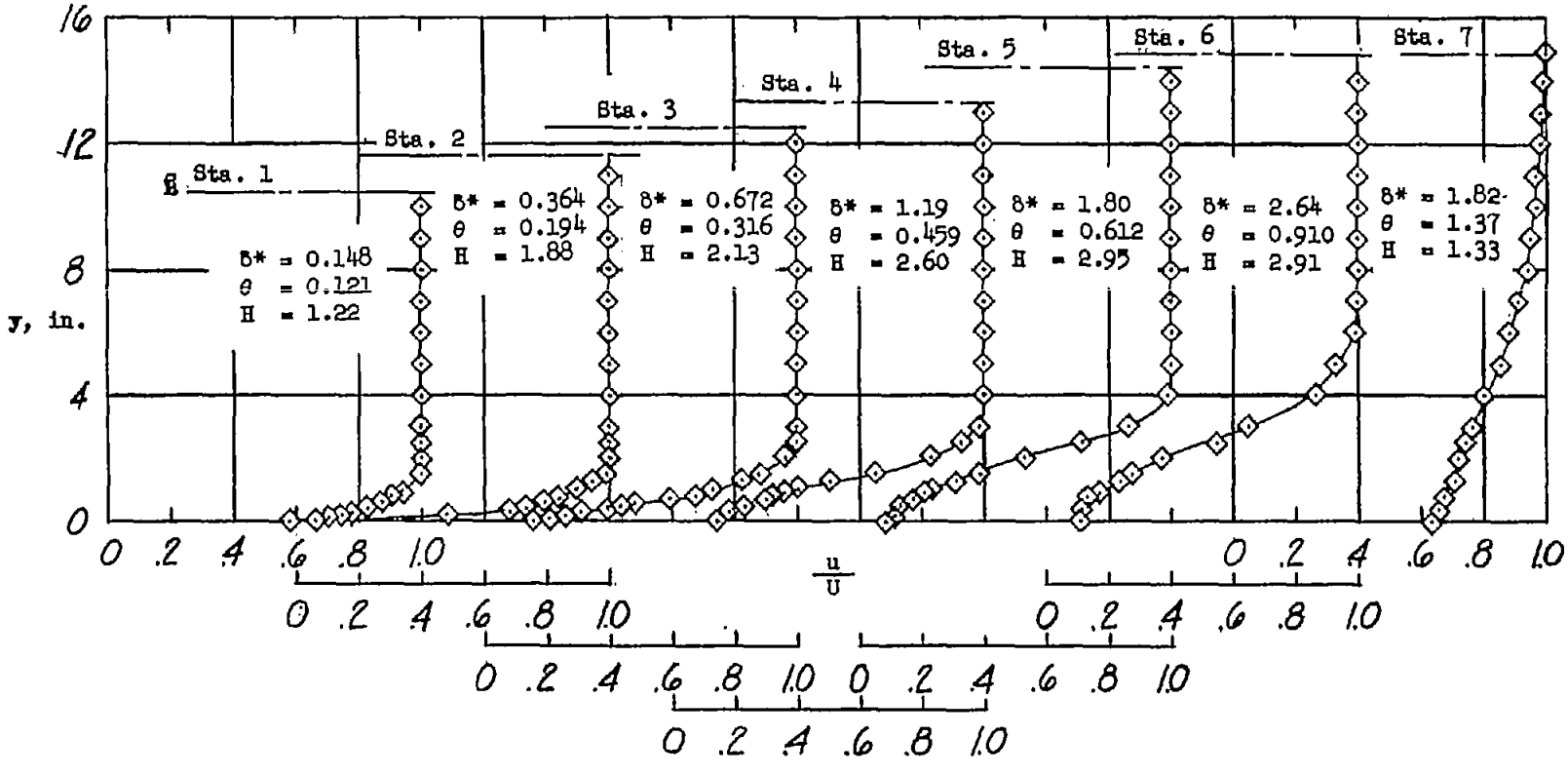

(c) $\frac{p_1}{p_0} \approx 0.915$.

Figure 9.- Concluded.

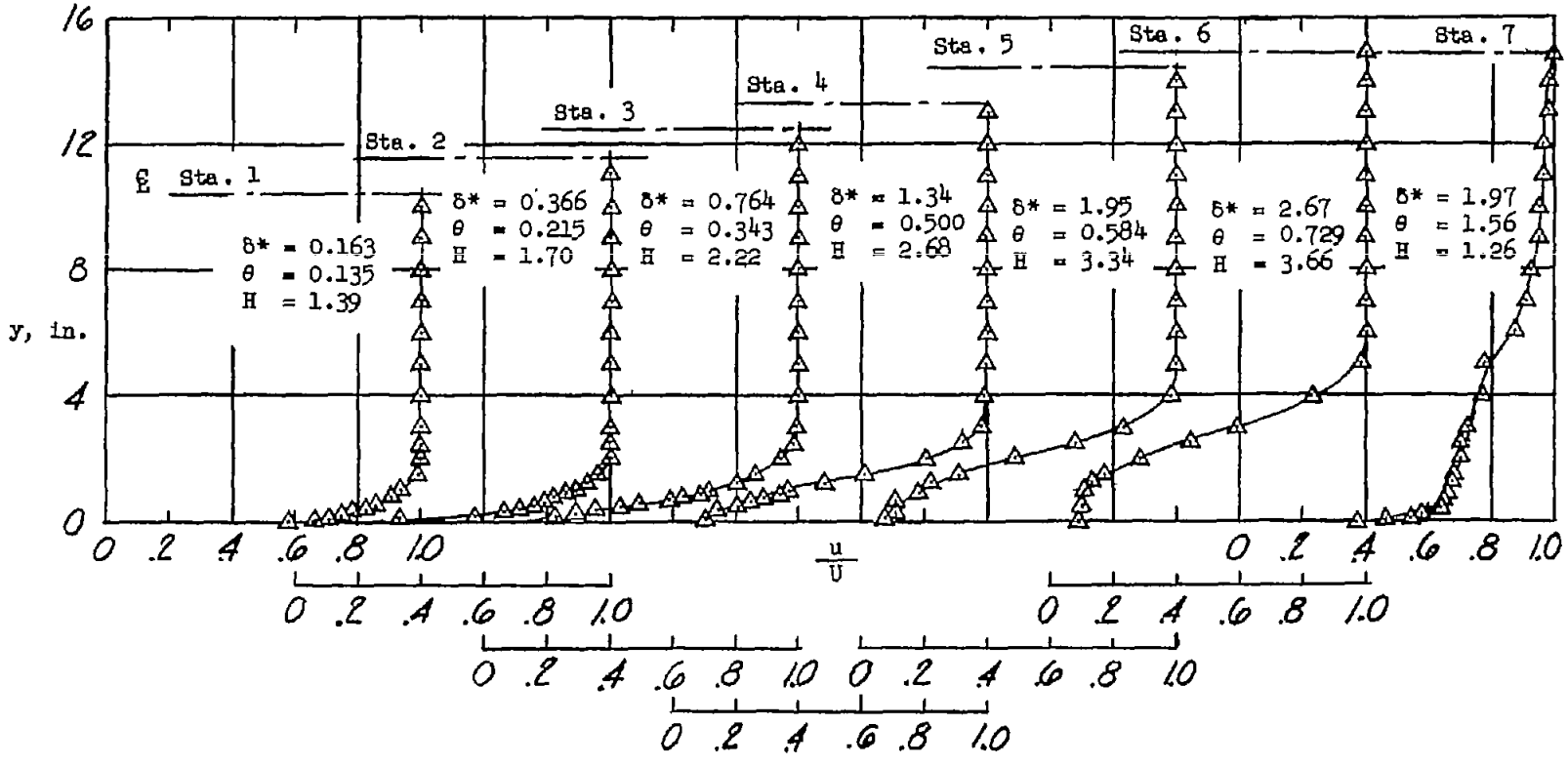

(a) $\frac{p_1}{p_0} \approx 0.96$.

Figure 10.- Boundary-layer velocity profiles along diffuser and at tailpipe exit for 86 percent of diffuser length roughened (configuration V).

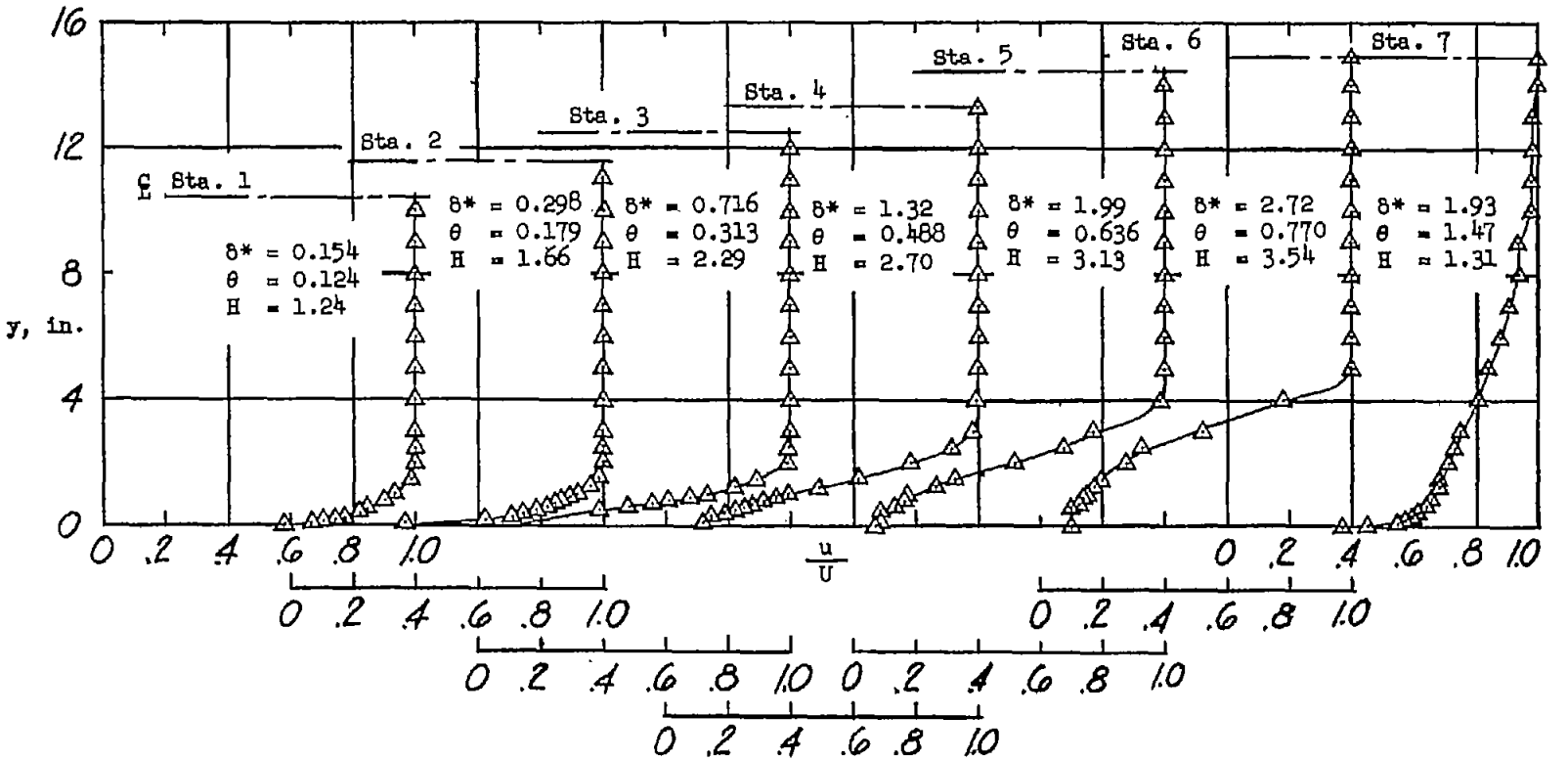

(b) $\frac{p_1}{p_0} \approx 0.94$.

Figure 10.- Continued.

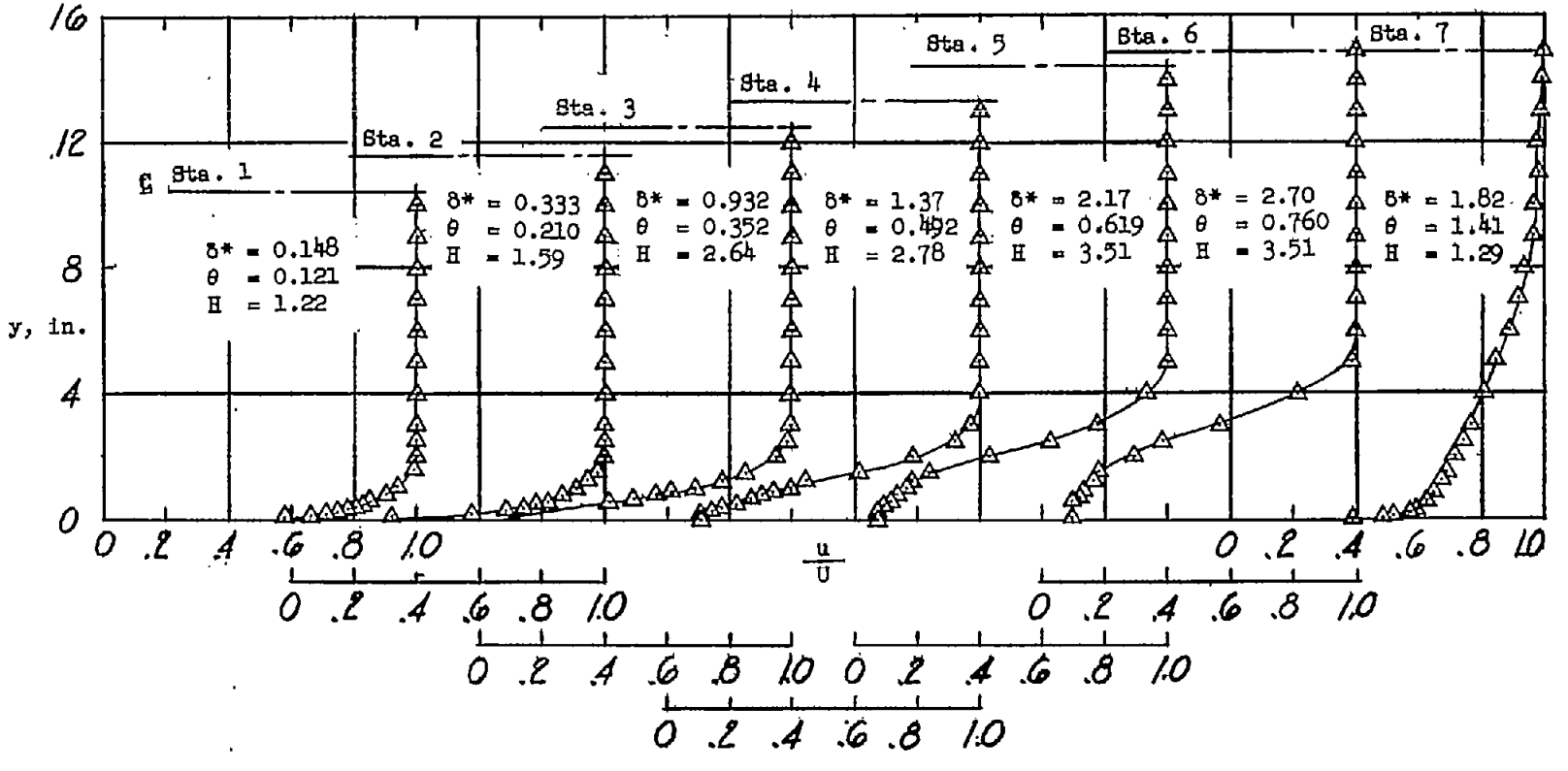

(c) $\frac{p_1}{p_0} \approx 0.915$.

Figure 10.- Concluded.

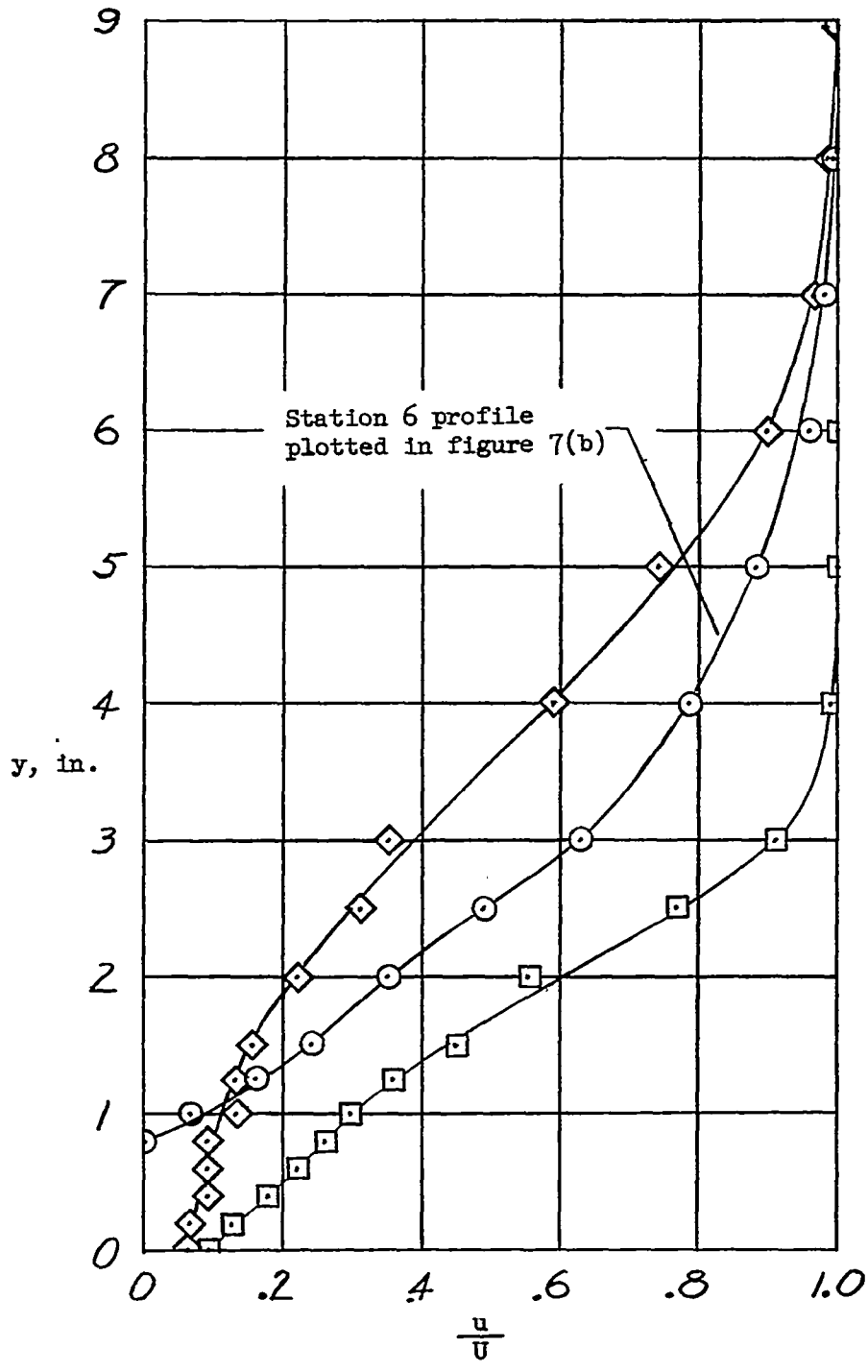

(a) 32 percent of diffuser length roughened (configuration VIII).

Figure 11.- Boundary-layer profiles 120° apart on circumference at diffuser exit, station 6, for $p_1/p_0 \approx 0.94$.

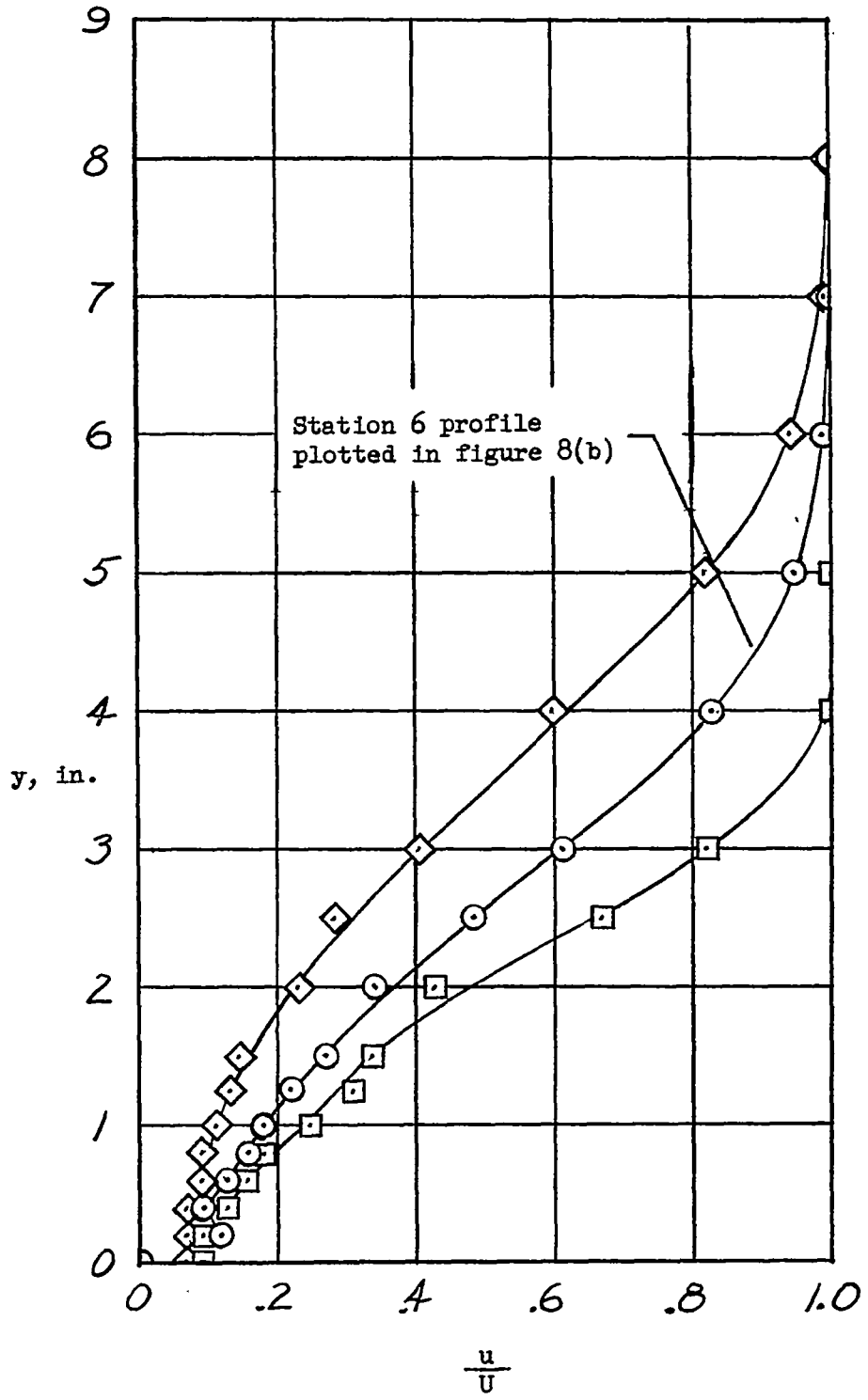

(b) 54 percent of diffuser length roughened (configuration VII).

Figure 11.- Continued.

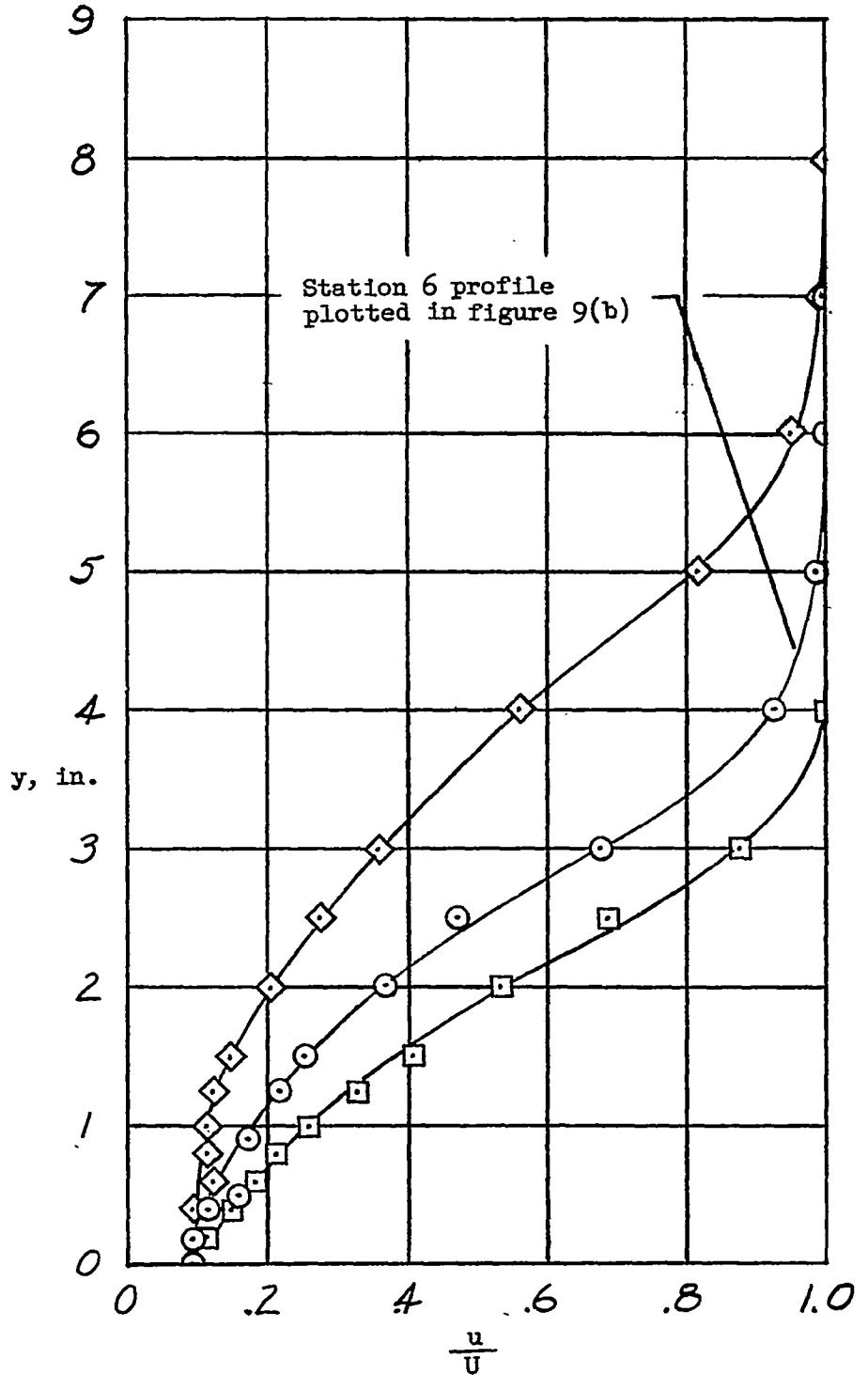

(c) 70 percent of diffuser length roughened (configuration VI).

Figure 11.- Continued.

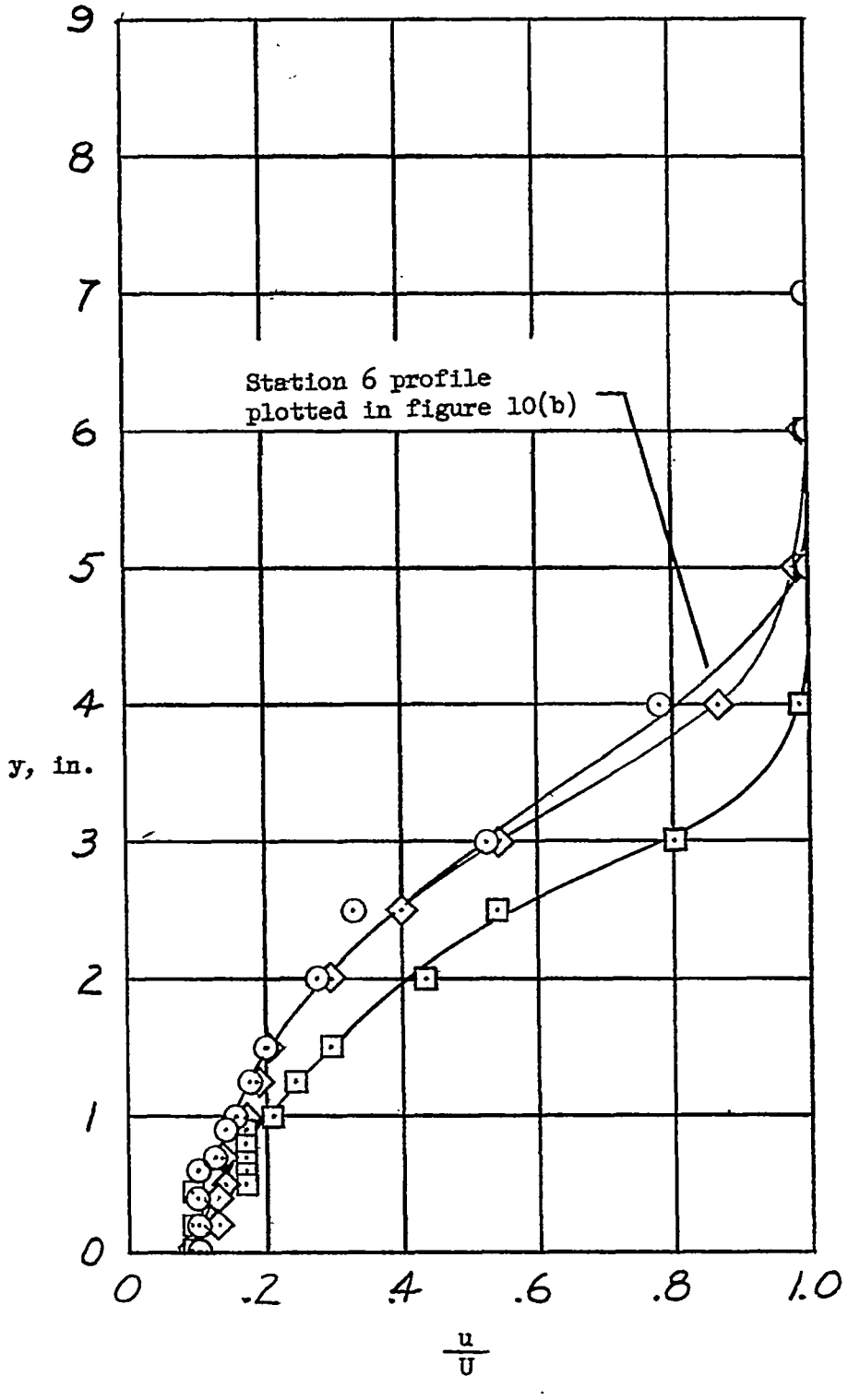

(d) 86 percent of diffuser length roughened (configuration V).

Figure 11.- Concluded.

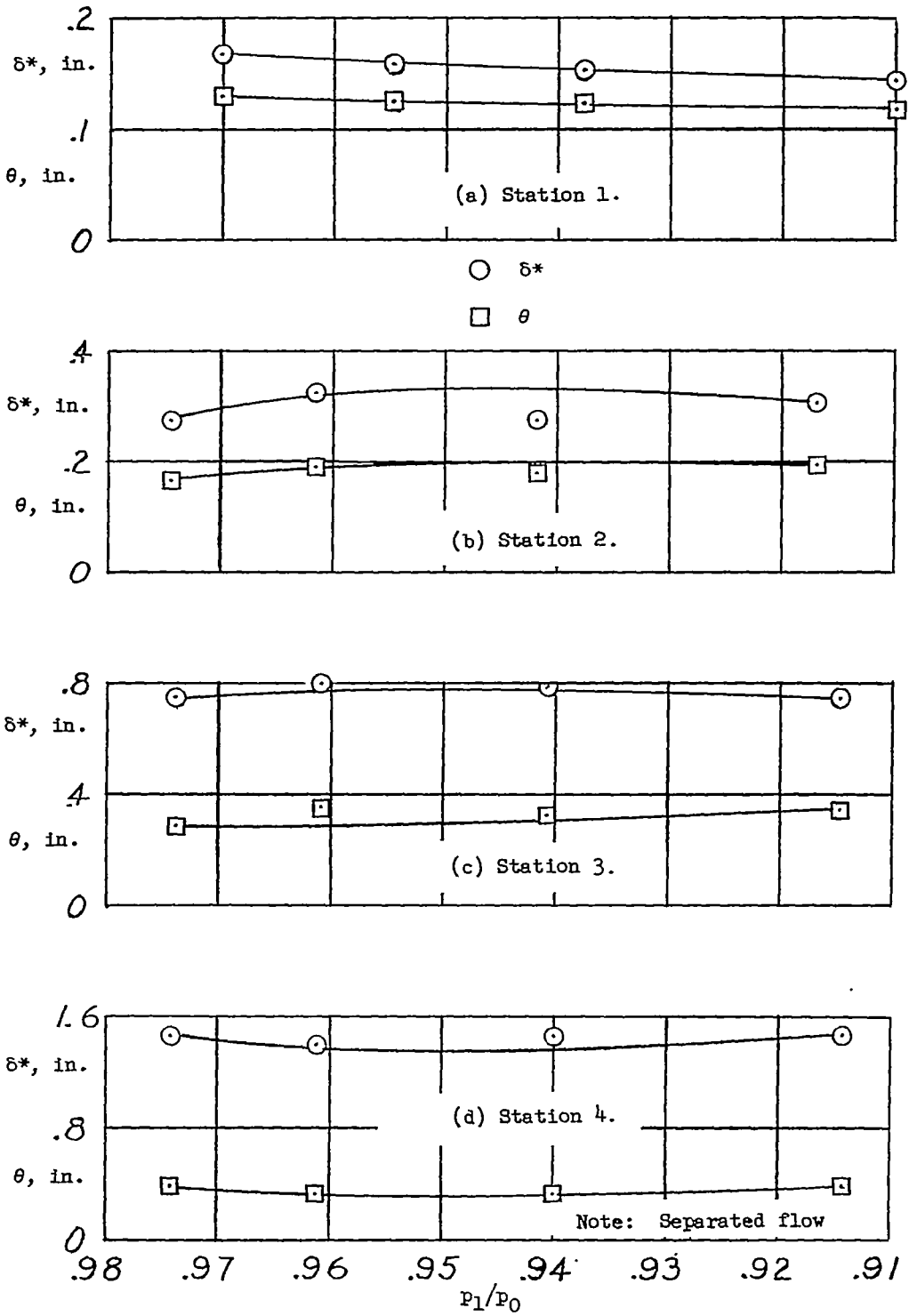

Figure 12.- Boundary-layer displacement and momentum thicknesses plotted against inlet pressure ratio for 32 percent of diffuser length roughened (configuration VIII).

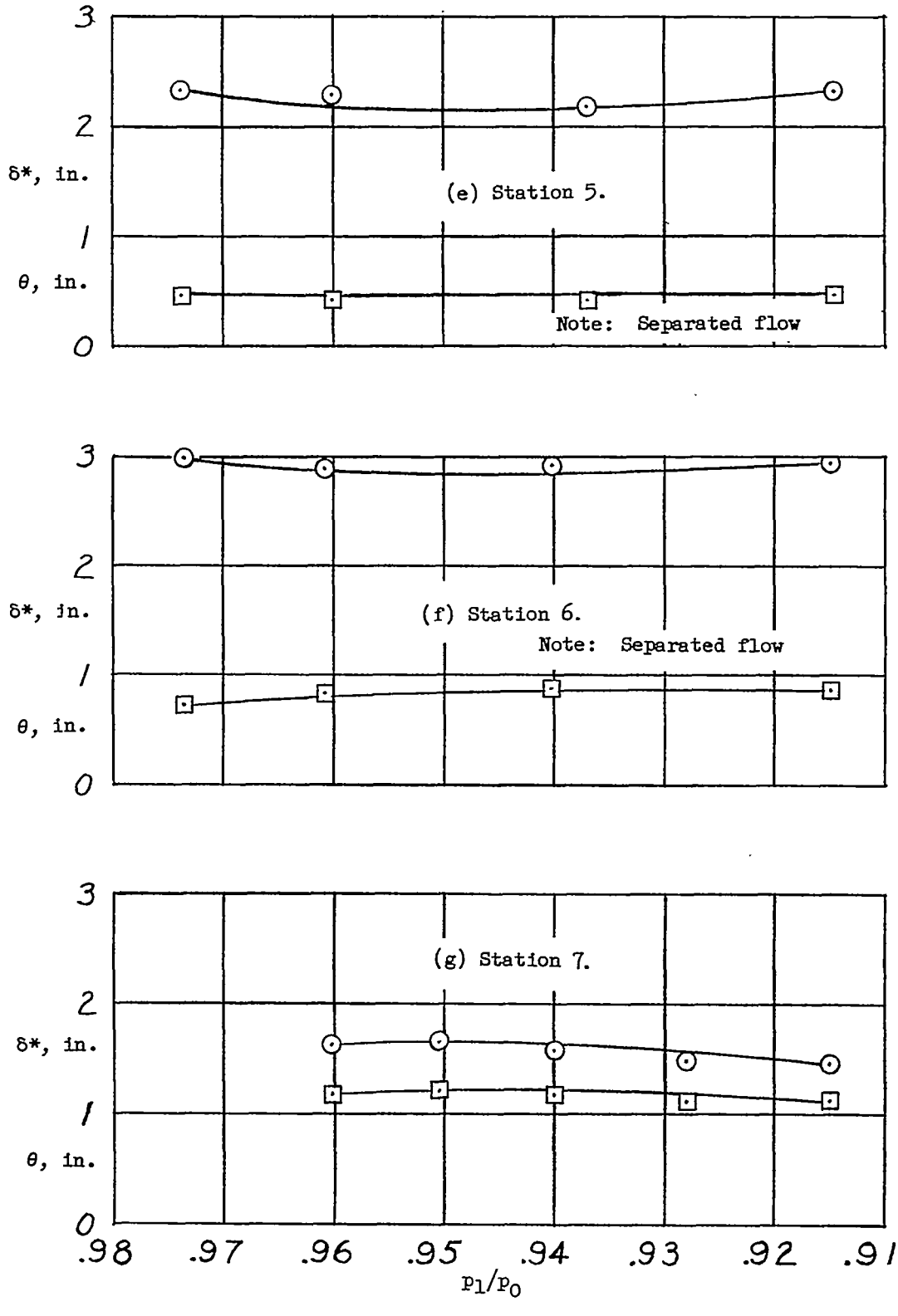

Figure 12.- Concluded.

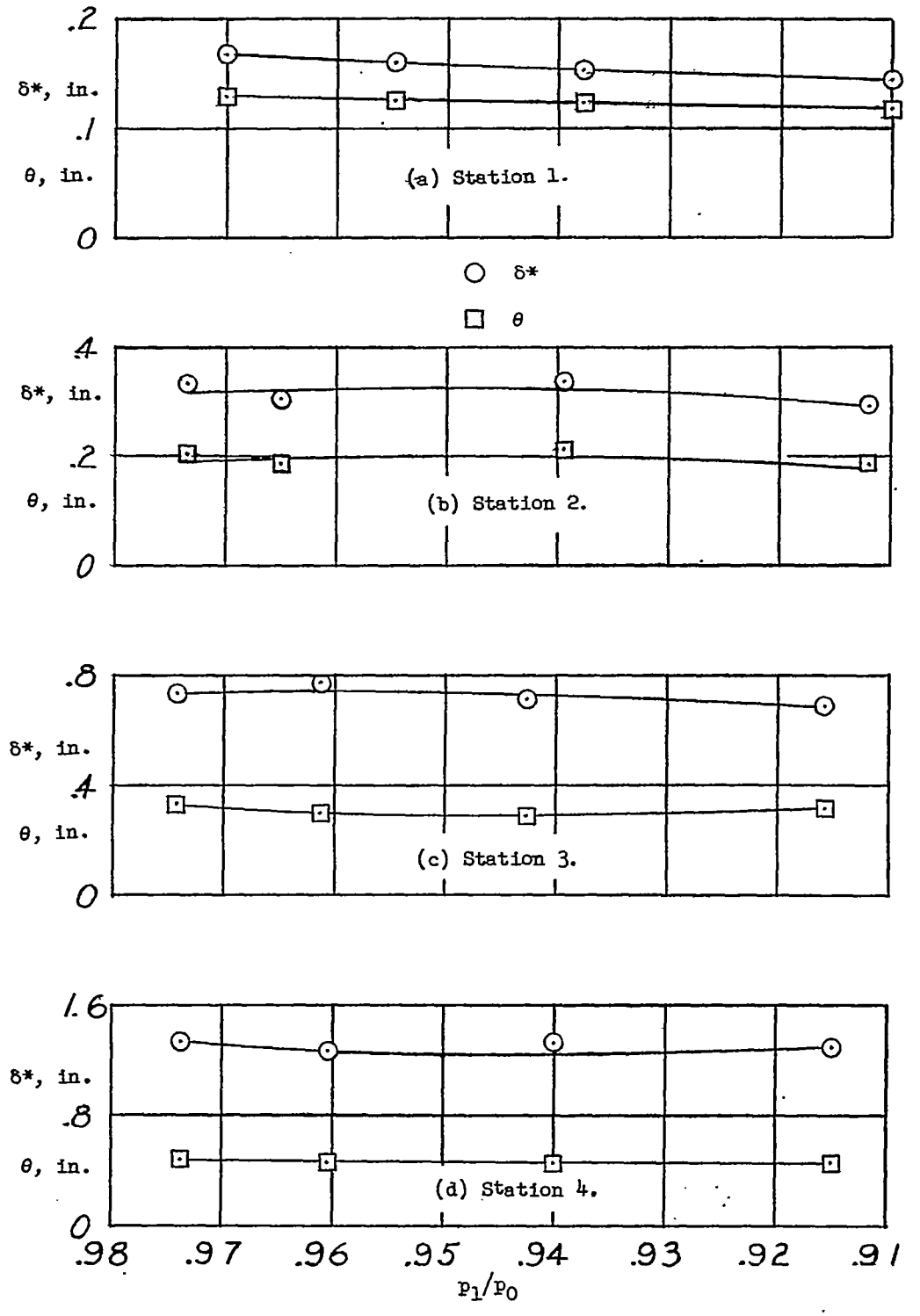

Figure 13.- Boundary-layer displacement and momentum thicknesses plotted against inlet pressure ratio for 54 percent of diffuser length roughened (configuration VII).

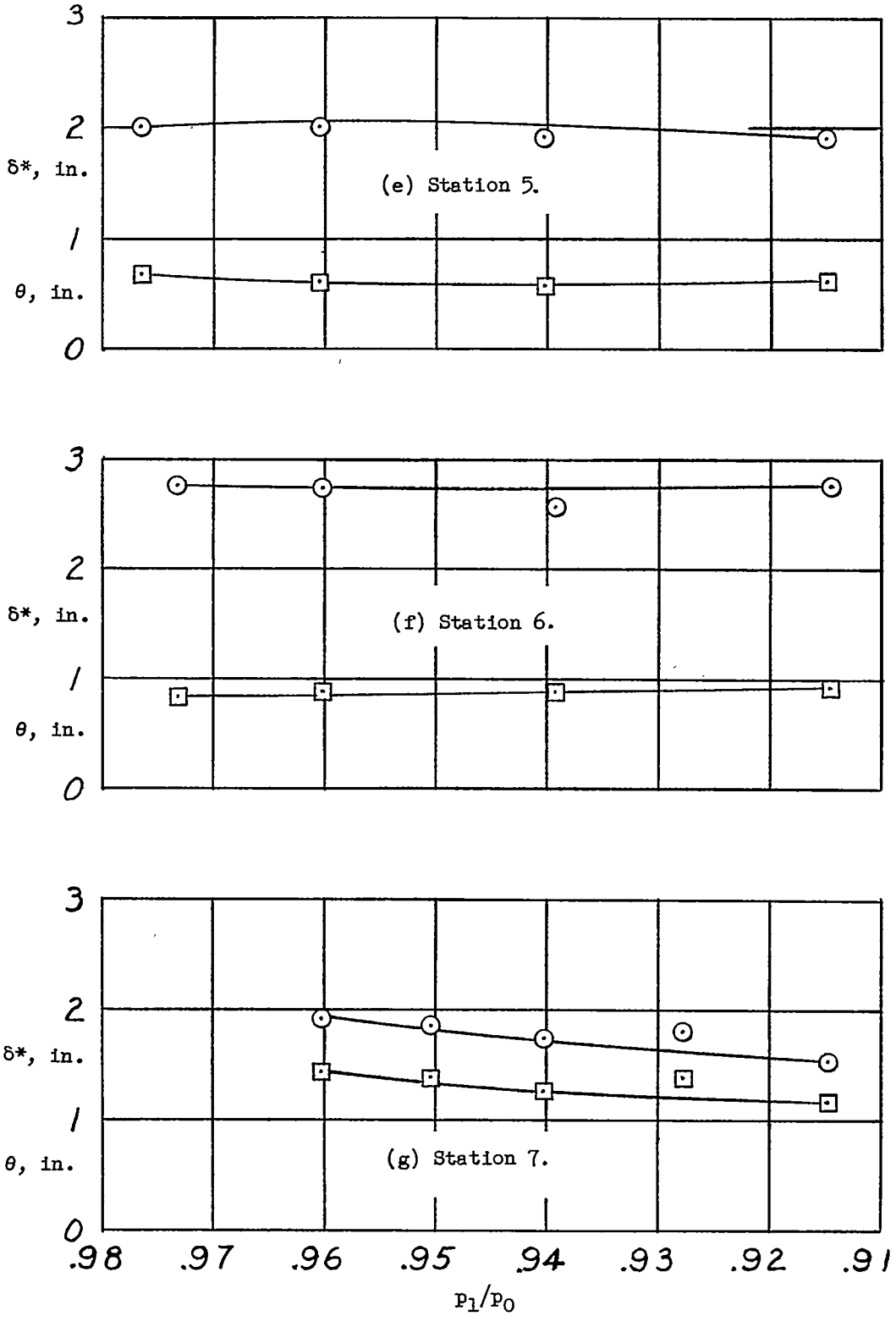

Figure 13.- Concluded.

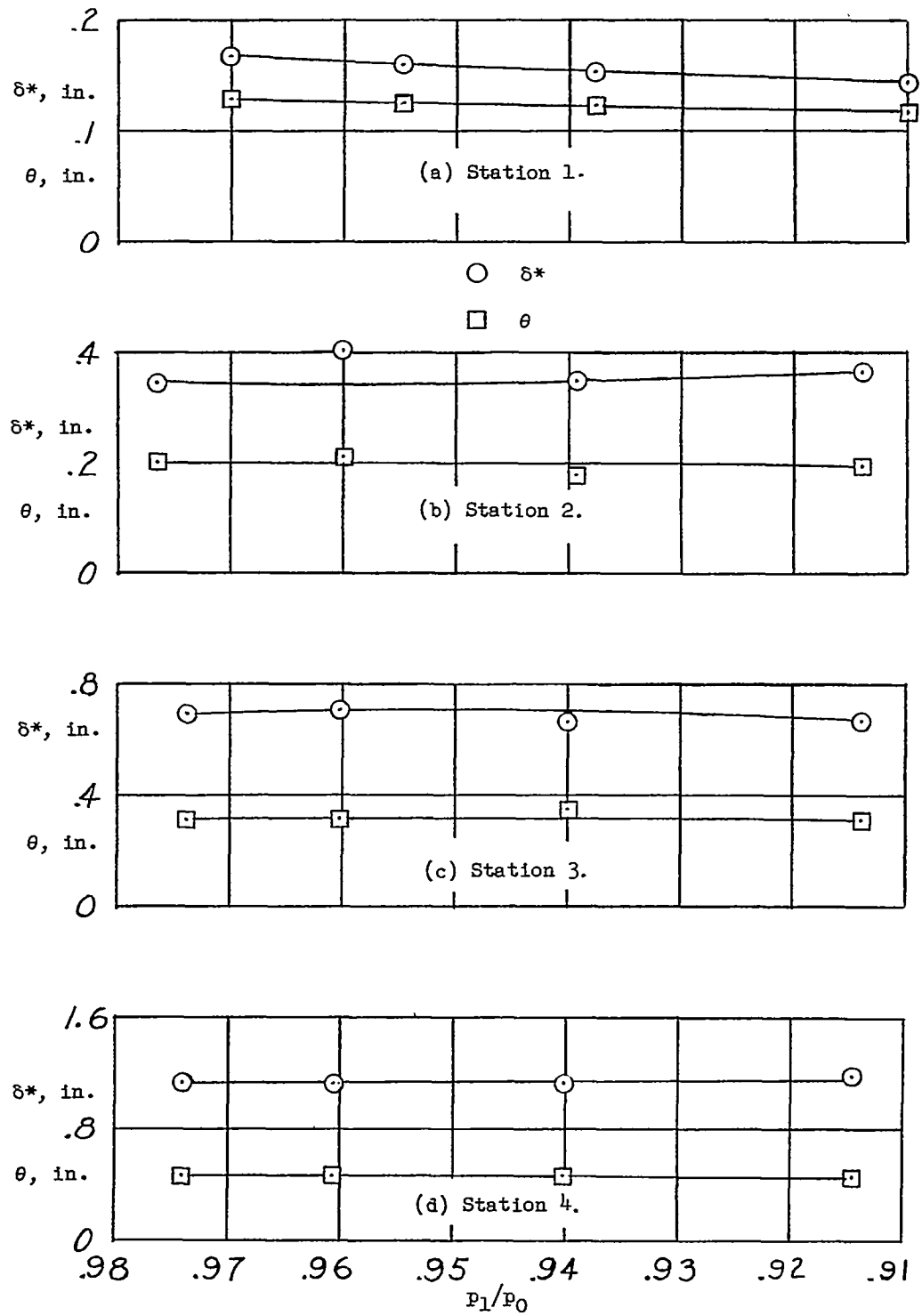

Figure 14.- Boundary-layer displacement and momentum thicknesses plotted against inlet pressure ratio for 70 percent of diffuser length roughened (configuration VI).

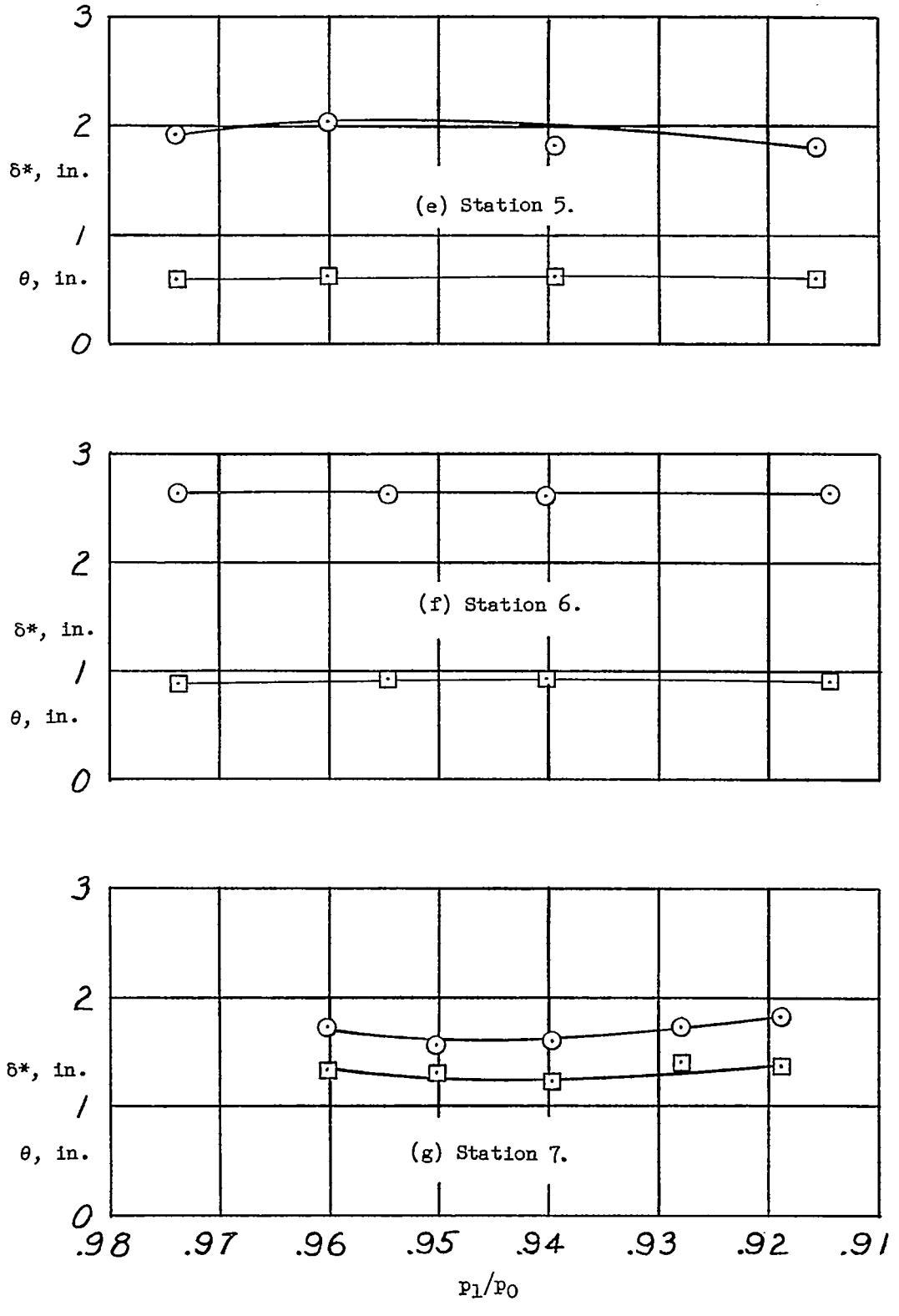

Figure 14.- Concluded.

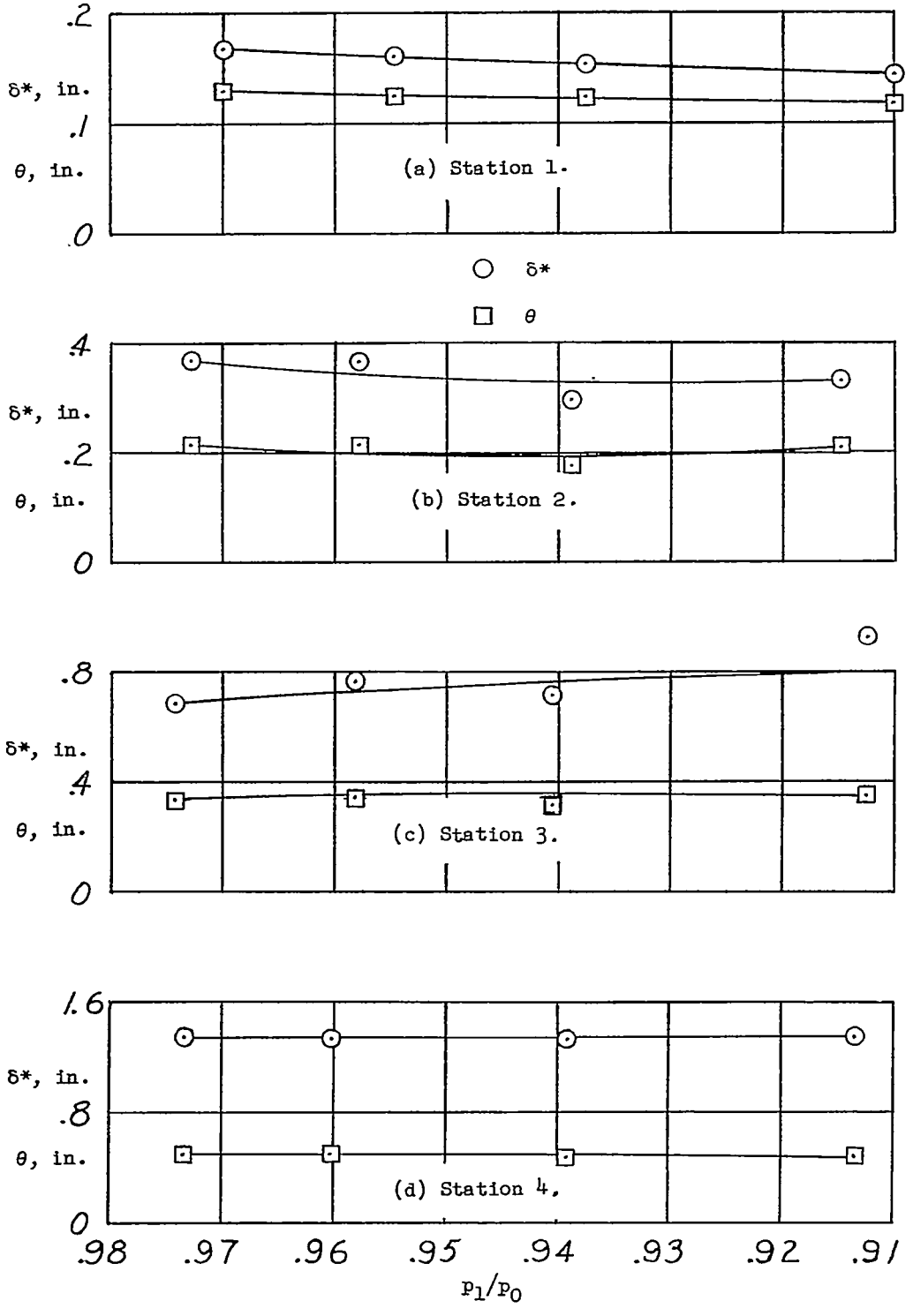

Figure 15.- Boundary-layer displacement and momentum thicknesses plotted against inlet pressure ratio for 86 percent of diffuser length roughened (configuration V).

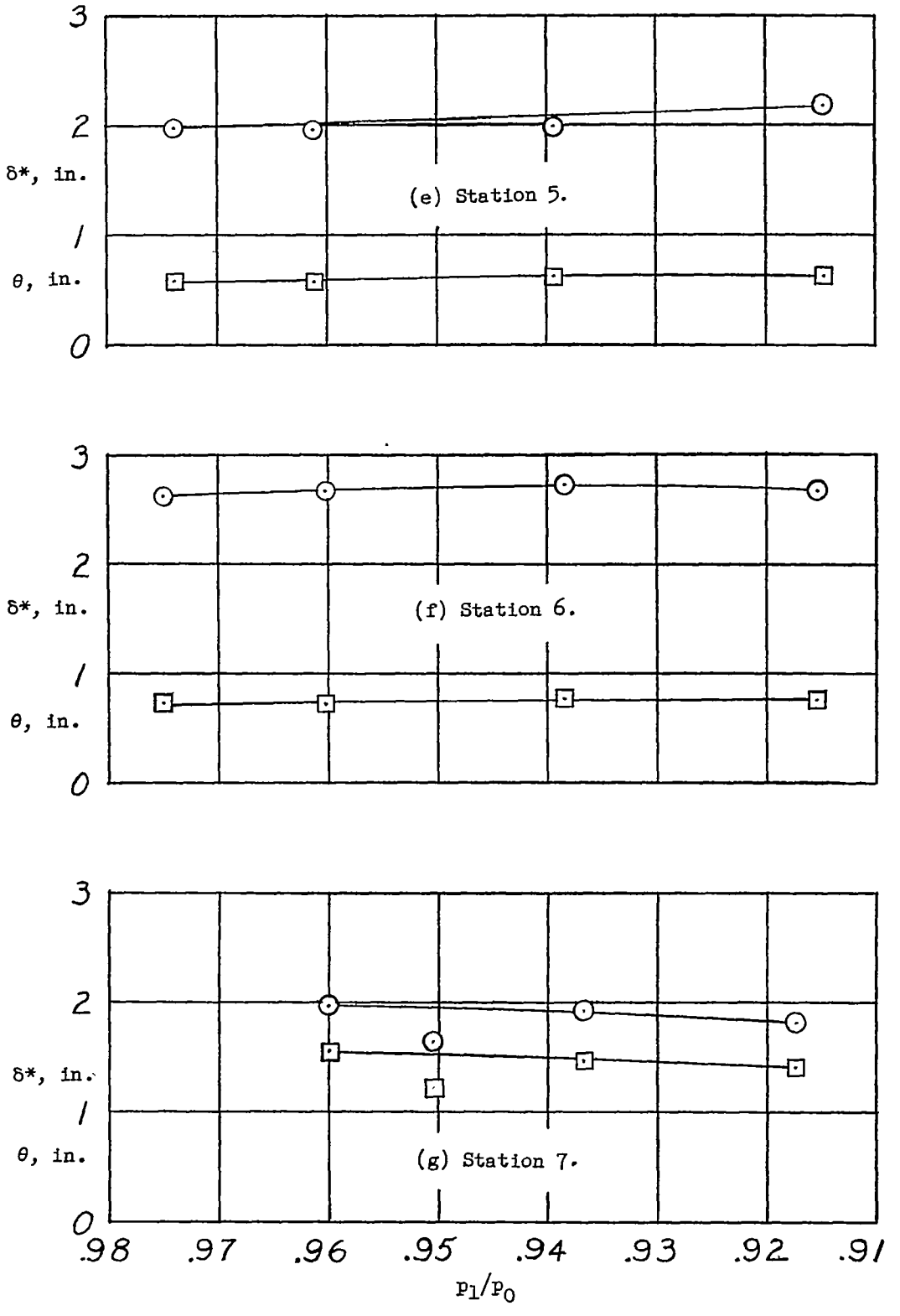

Figure 15.- Concluded.

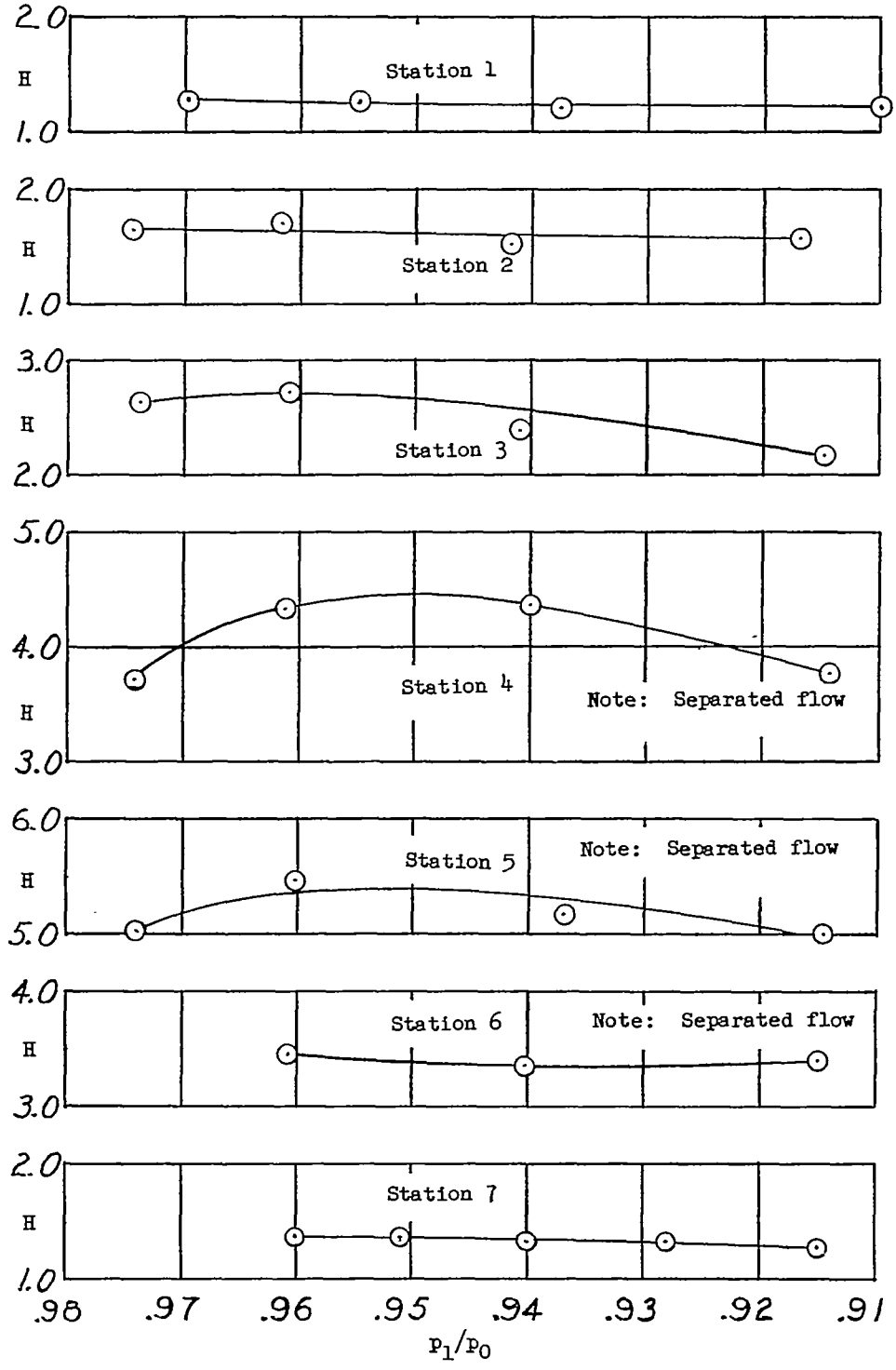

(a) 32 percent of diffuser length roughened (configuration VIII).

Figure 16.- Variation of boundary-layer shape parameter with inlet pressure ratio.

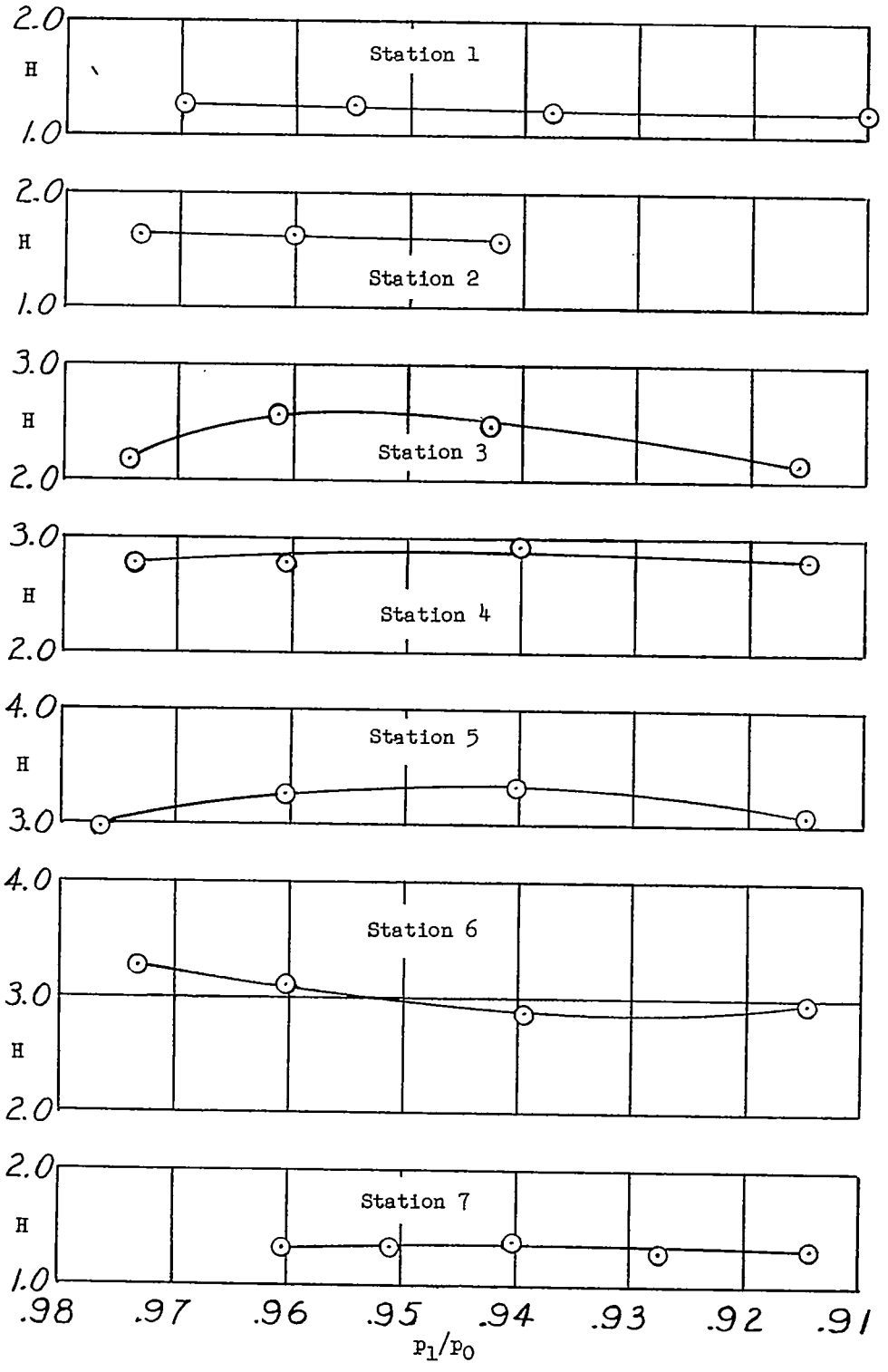

(b) 54 percent of diffuser length roughened (configuration VII).

Figure 16.- Continued.

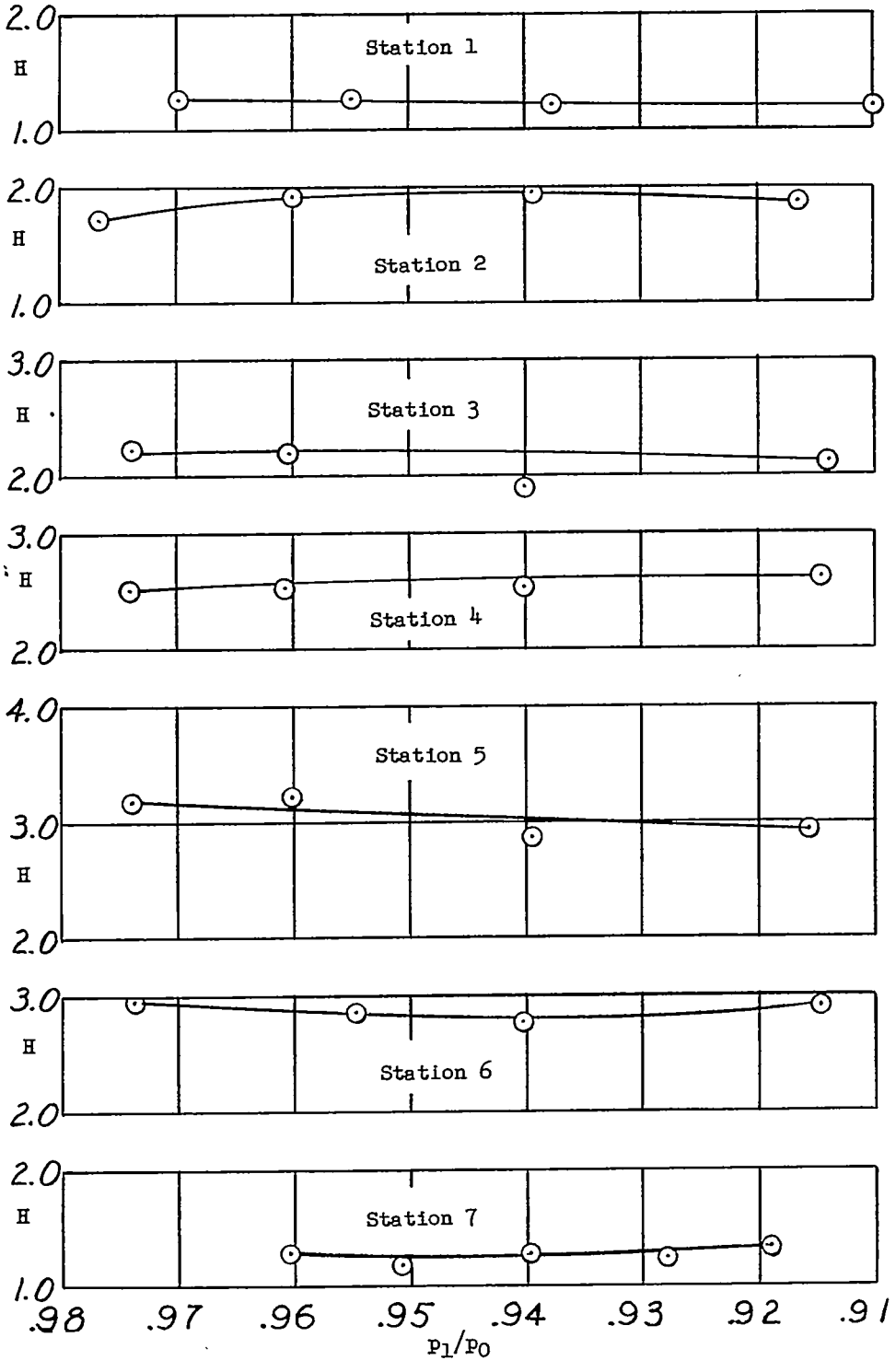

(c) 70 percent of diffuser length roughened (configuration VI).

Figure 16.- Continued.

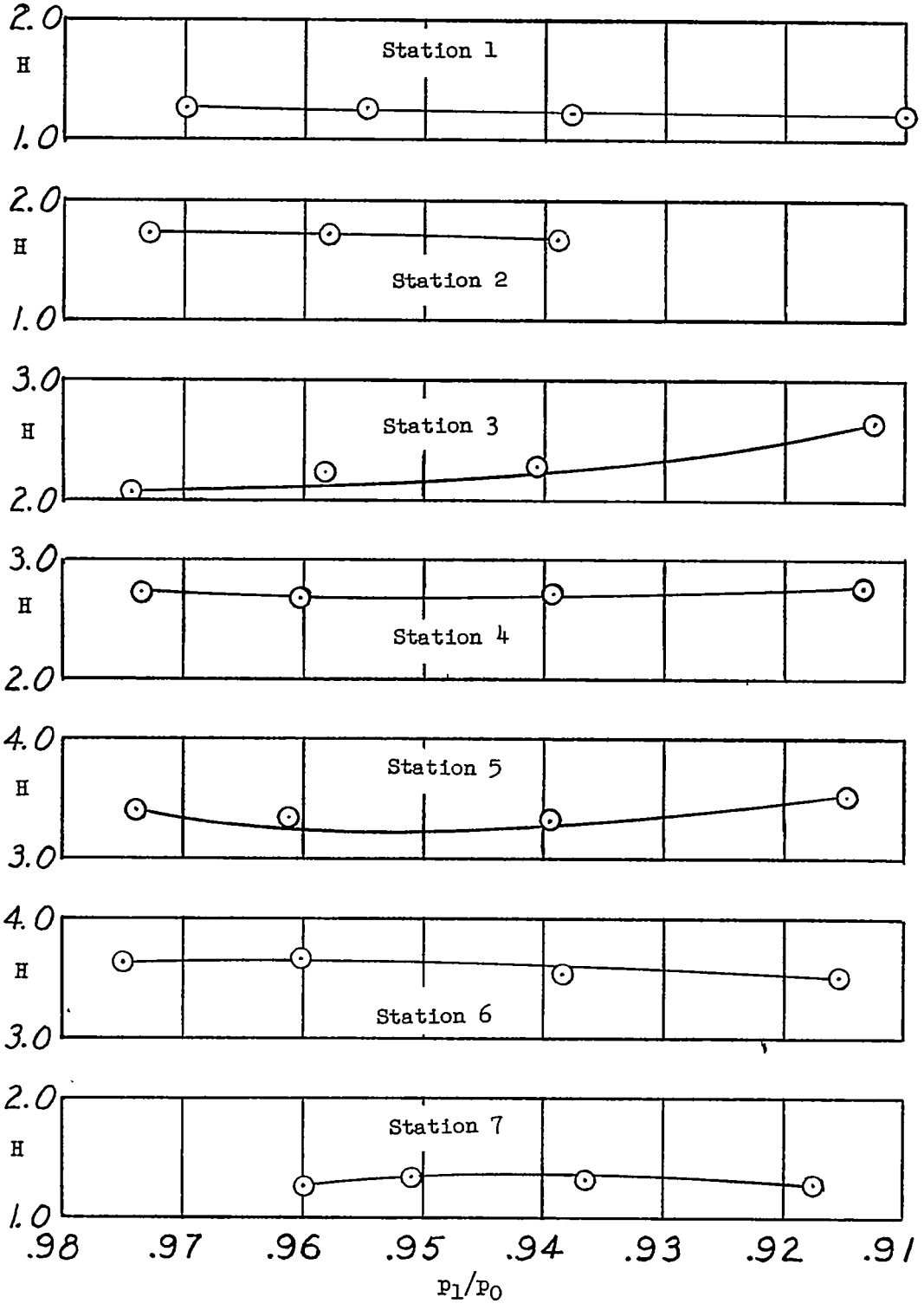

(d) 86 percent of diffuser length roughened (configuration V).

Figure 16.- Concluded.

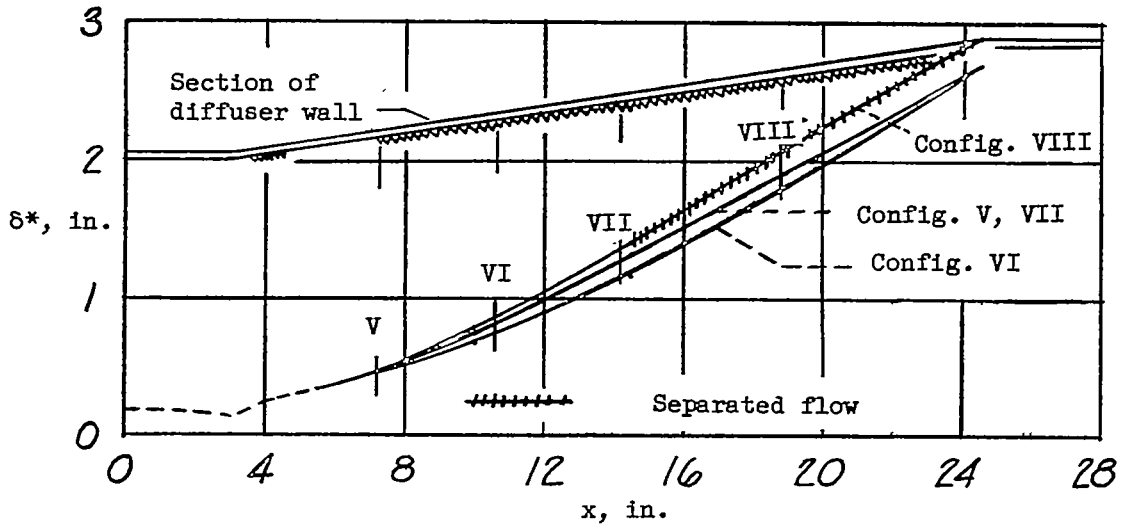

(a) Displacement thickness.

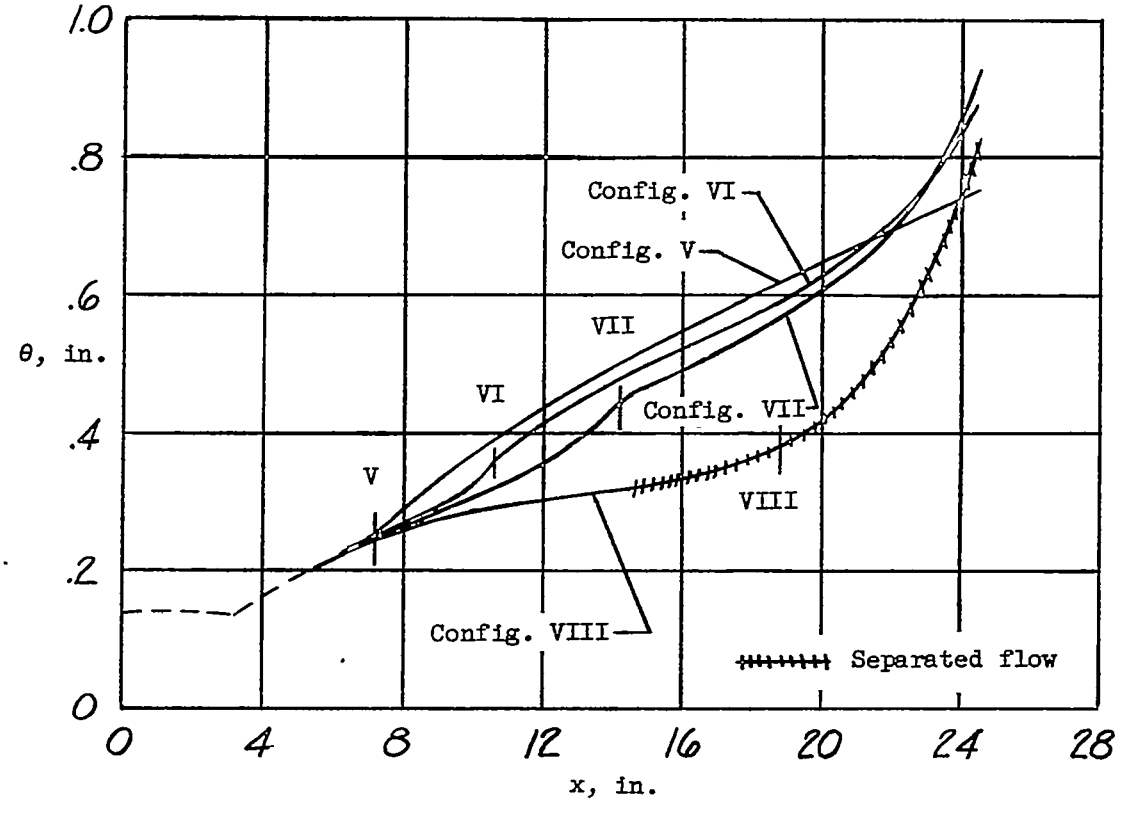

(b) Momentum thickness.

Figure 17.- Variation of boundary-layer parameters with distance along diffuser. $p_1/p_0 = 0.95$.

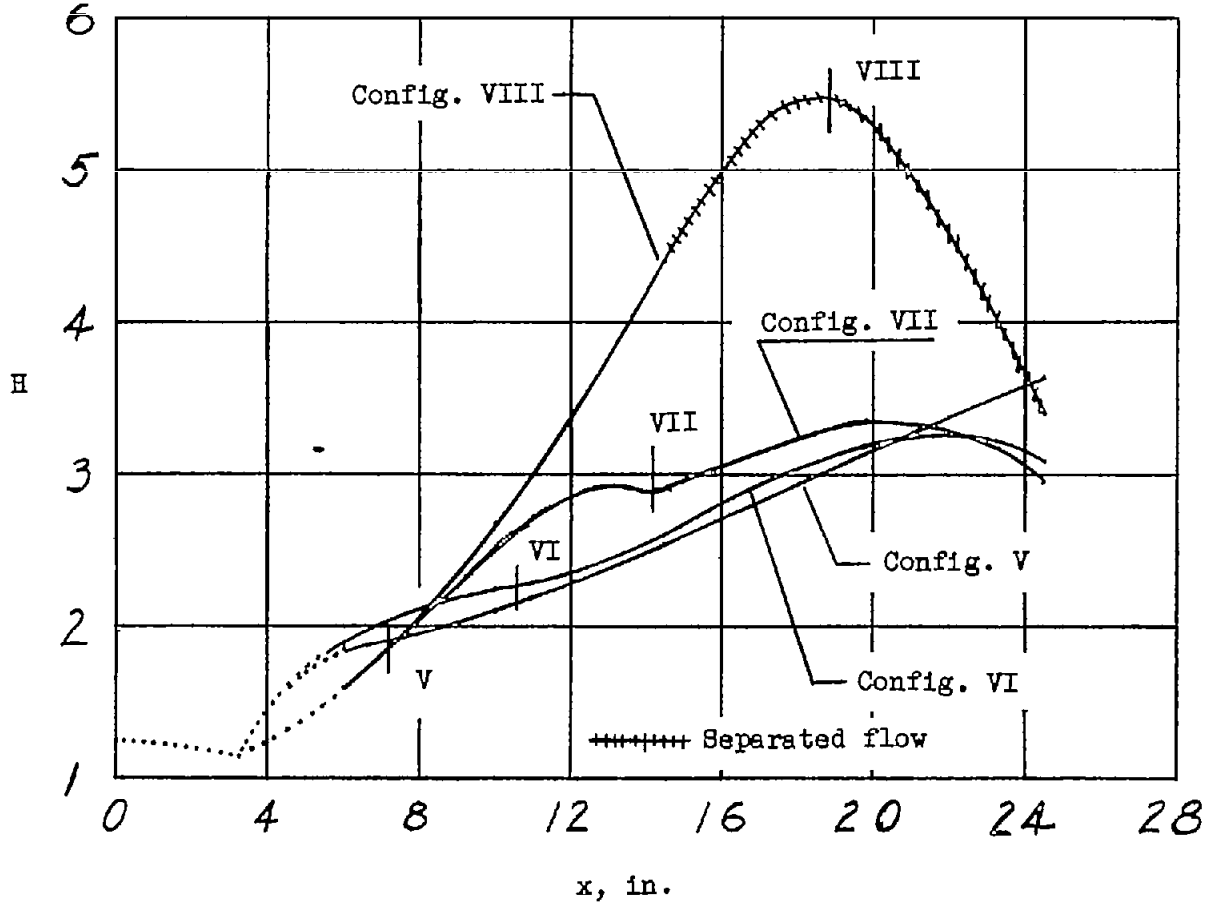

(c) Boundary-layer shape parameter.

Figure 17.- Concluded.

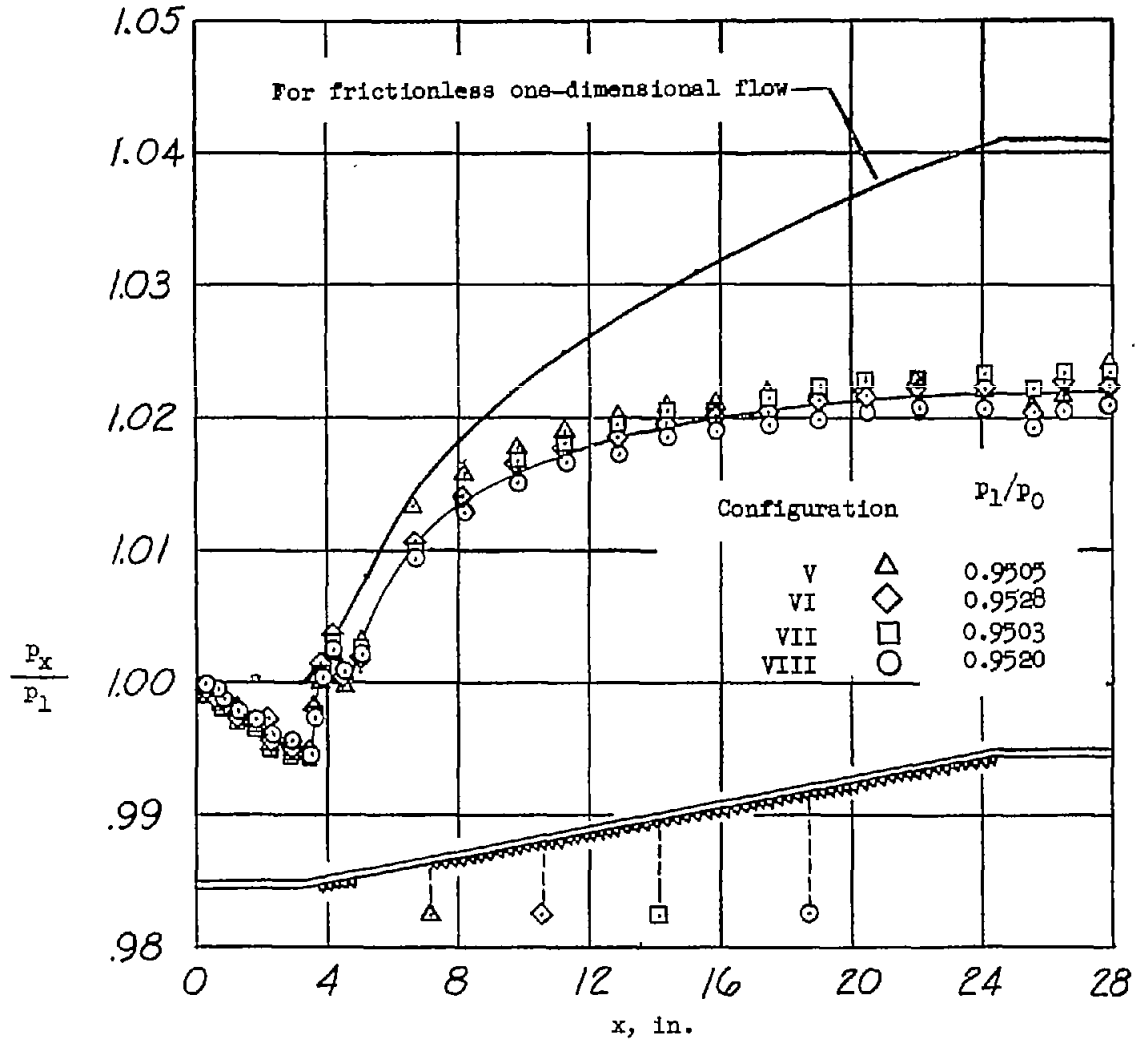

Figure 18.- Variation of ratio of longitudinal static pressure to inlet static pressure with distance along longitudinal axis for all configurations.

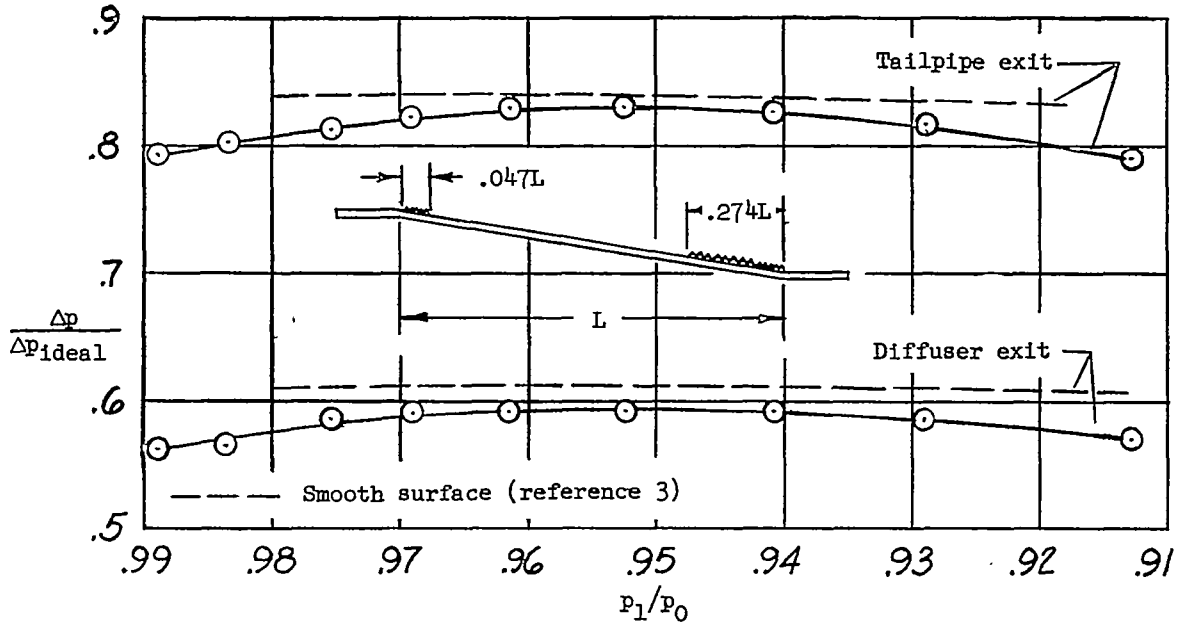

(a) 32 percent of diffuser length roughened (configuration VIII).

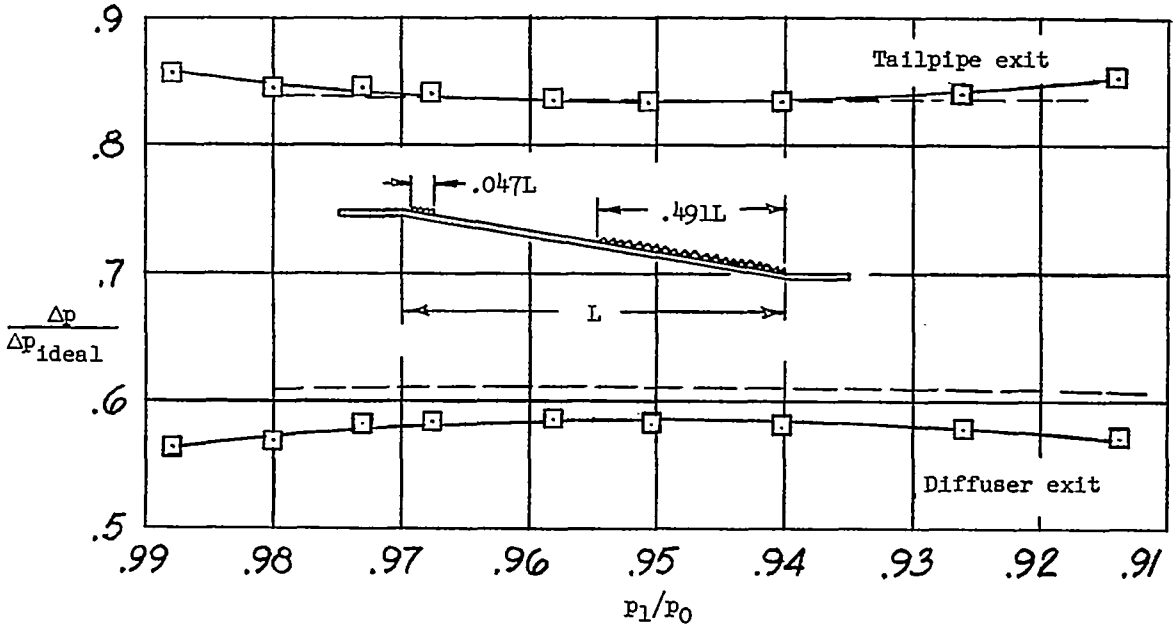

(b) 54 percent of diffuser length roughened (configuration VII).

Figure 19.- Variation of diffuser effectiveness with inlet pressure ratio for rough-surface configurations.

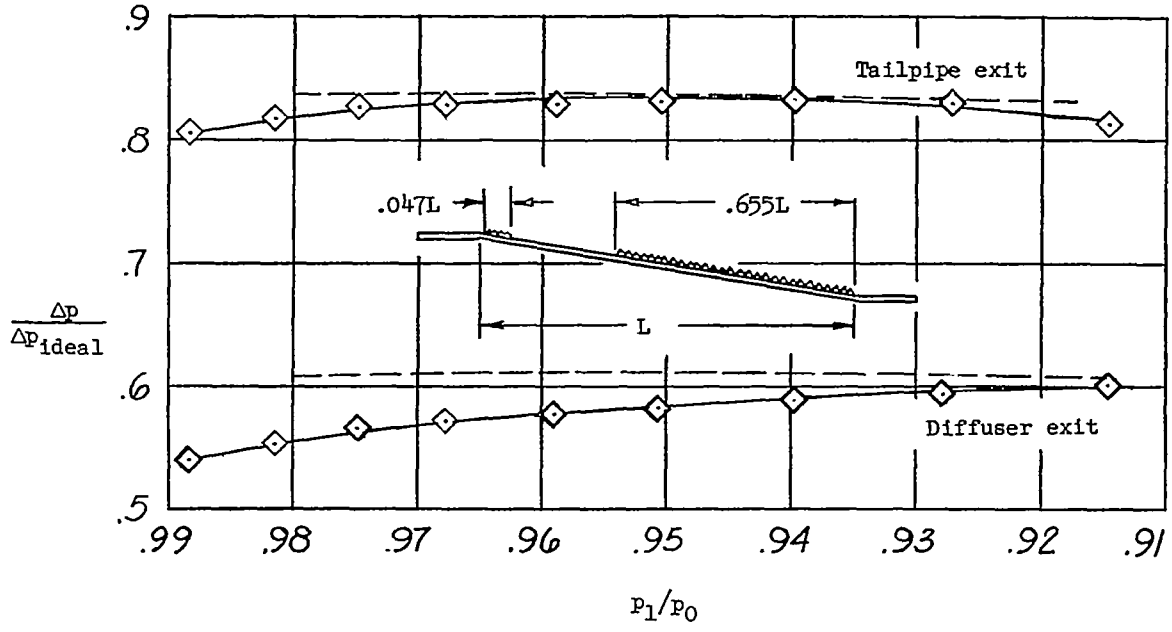

(c) 70 percent of diffuser length roughened (configuration VI).

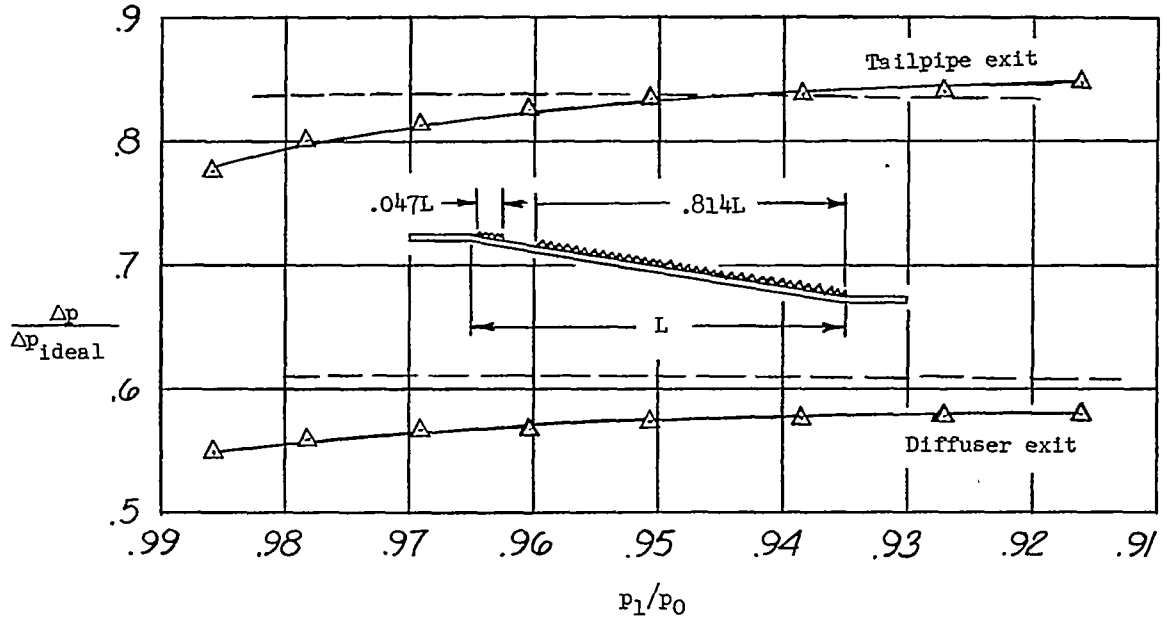

(d) 86 percent of diffuser length roughened (configuration V).

Figure 19.- Concluded.

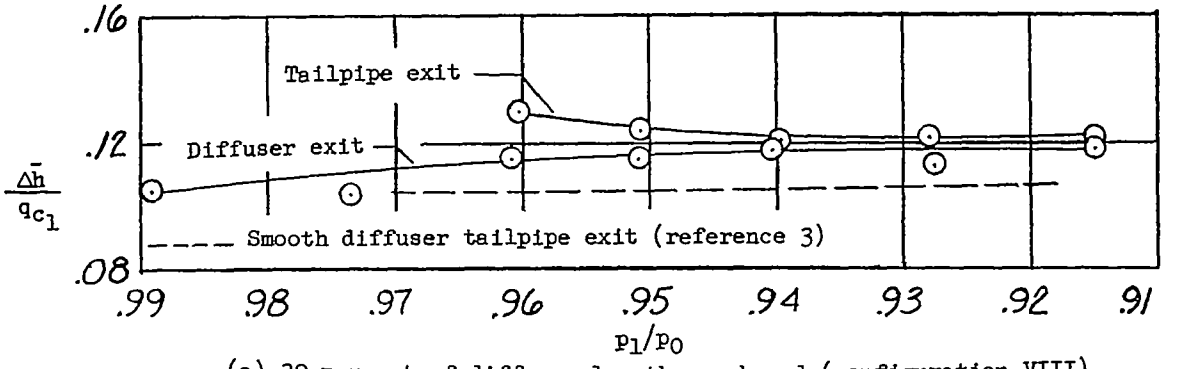

(a) 32 percent of diffuser length roughened (configuration VIII).

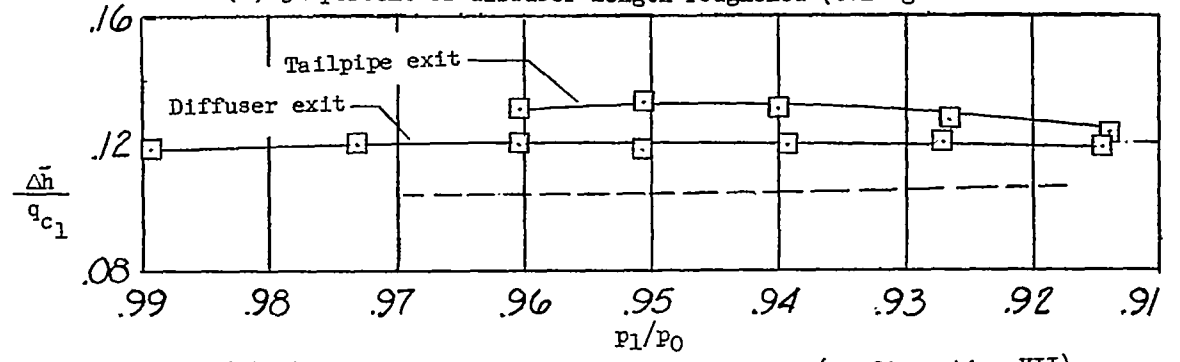

(b) 54 percent of diffuser length roughened (configuration VII).

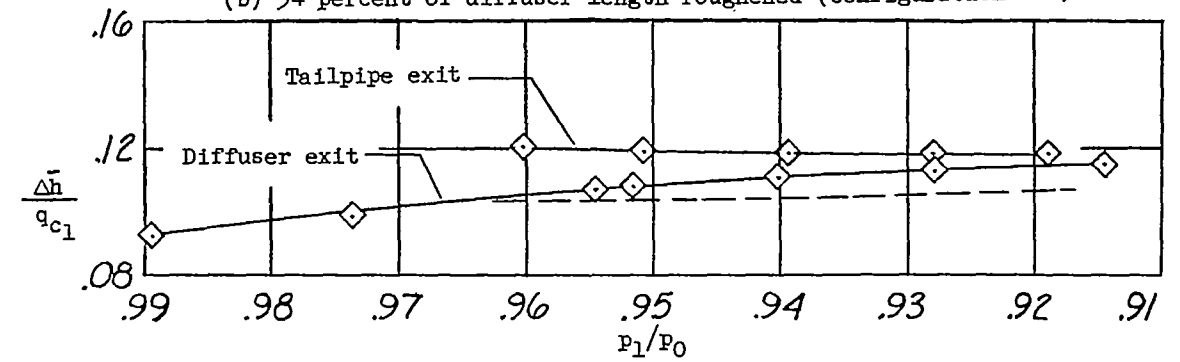

(c) 70 percent of diffuser length roughened (configuration VI).

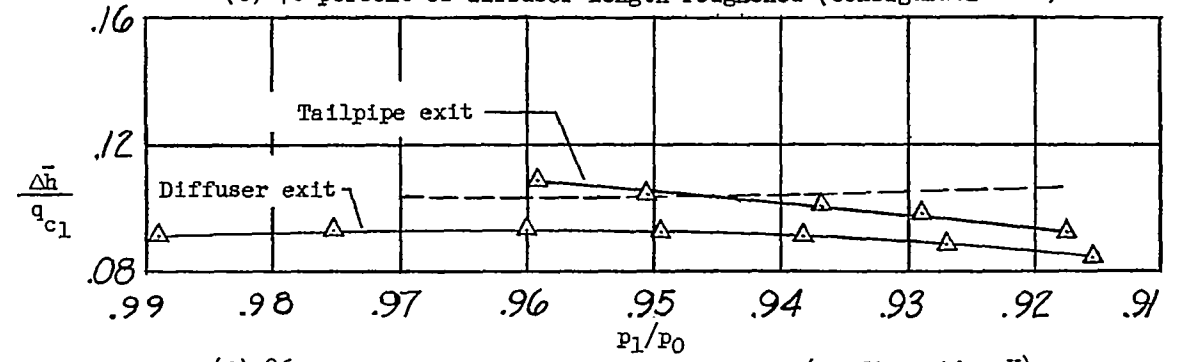

(d) 86 percent of diffuser length roughened (configuration V).

Figure 20.- Total-pressure-loss coefficient plotted against inlet pressure ratio.

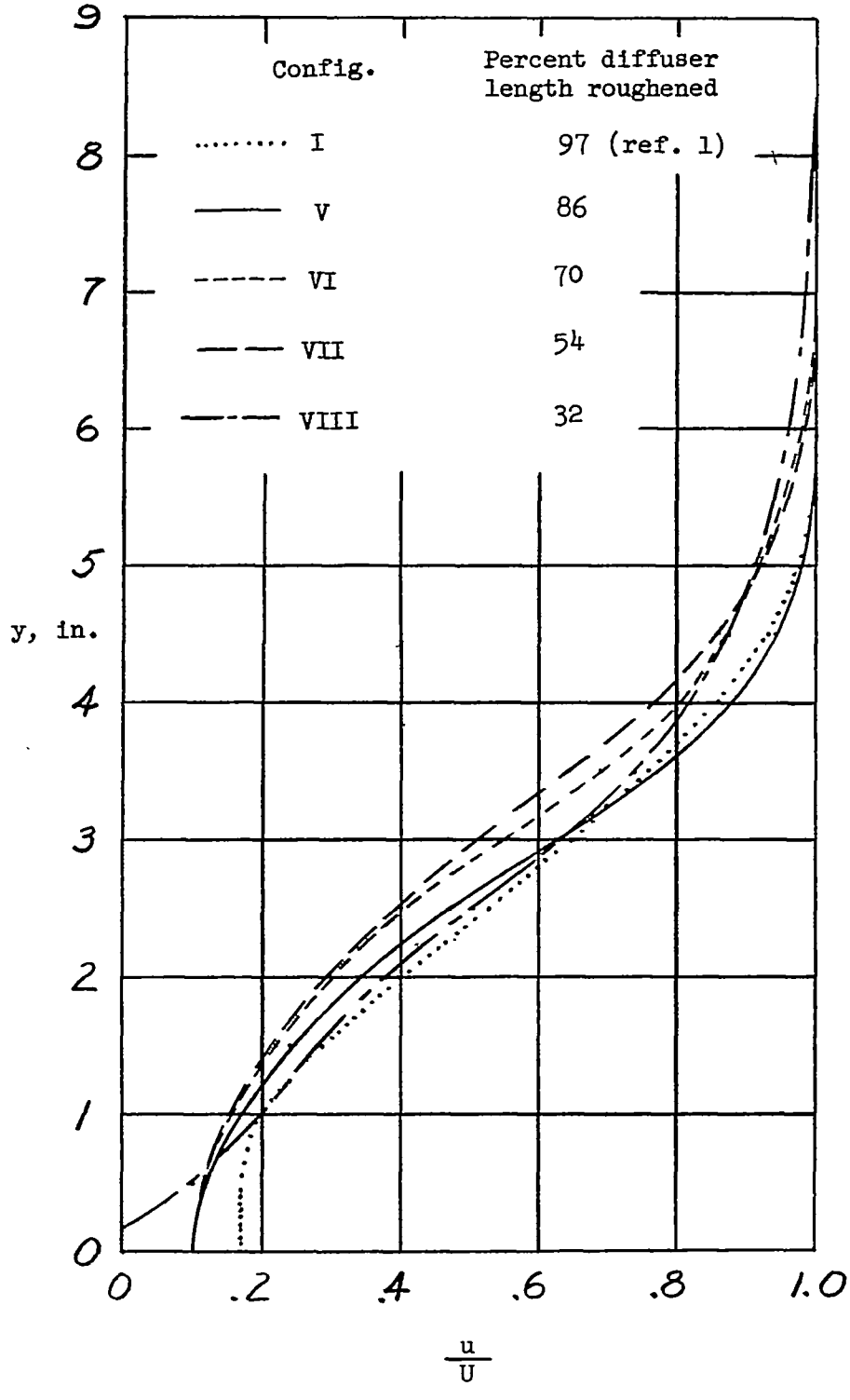

Figure 21.- Boundary-layer velocity profiles at diffuser exit, station 6, for all configurations. $p_1/p_0 = 0.95$.

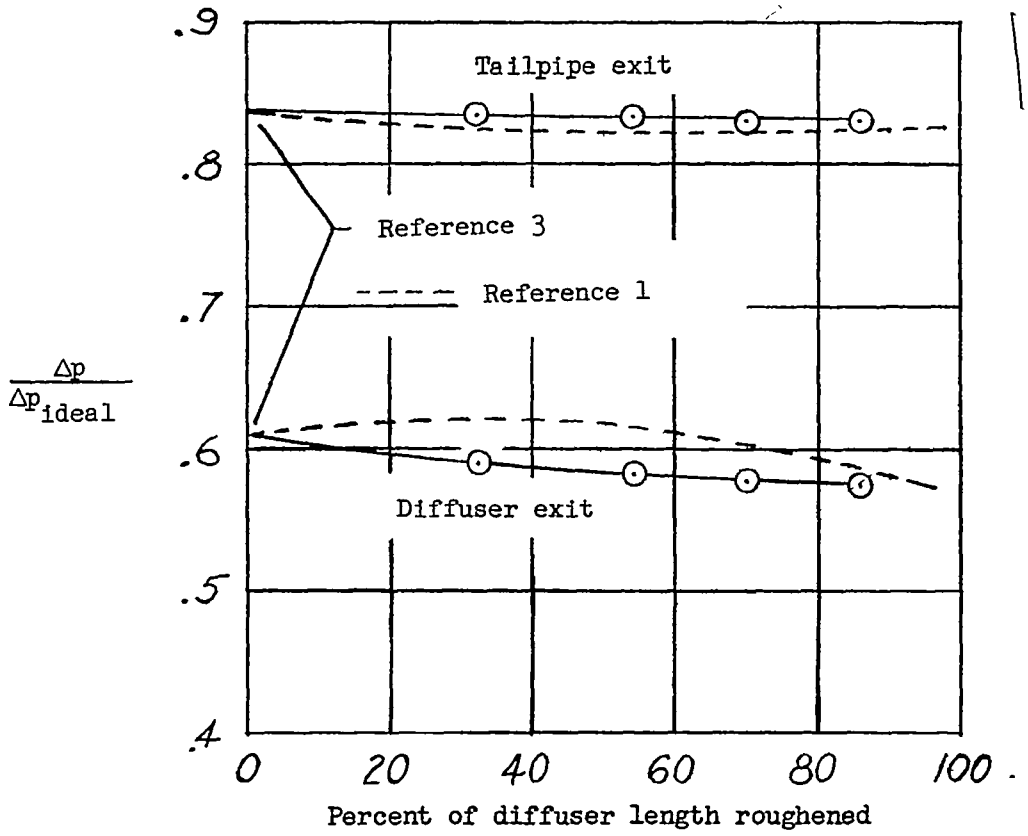

(a) Diffuser effectiveness.

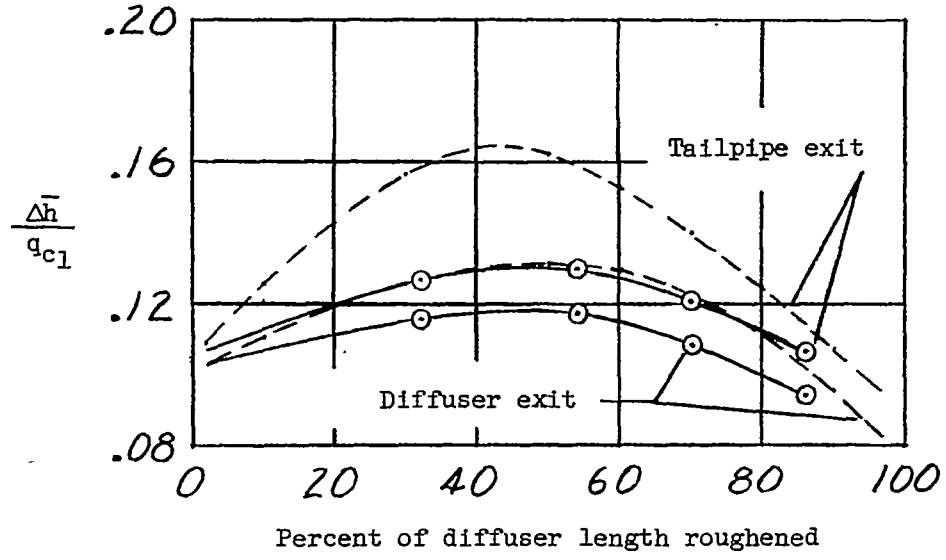

(b) Total-pressure-loss coefficient.

Figure 22.- Variation of performance parameters with extent of surface roughness for $p_1/p_0 = 0.95$.

NACA-Langley - 1-22-54 - 1000